Sneutrino-induced like sign dilepton signal with conserved R-parity

St. Kolb, M. Hirsch[†], H.V. Klapdor-Kleingrothaus[‡] and O. Panella

Istituto Nazionale di Fisica Nucleare, Sezione di Perugia, Via A. Pascoli, I-06123 Perugia, Italy
[†]*Department of Physics and Astronomy, University of Southampton, Highfield, Southampton SO17 1BJ, England*
[‡]*Max-Planck-Institut für Kernphysik, P.O. 10 39 80, D-69029 Heidelberg, Germany*

Abstract

Lepton number violation could be manifest in the sneutrino sector of supersymmetric extensions of the standard model with conserved R-parity. Then sneutrinos decay partly into the "wrong sign charged lepton" final state, if kinematically accessible. In sneutrino pair production or associated single sneutrino production, the signal then is a like sign dilepton final state. Under favourable circumstances, such a signal could be visible at the LHC or a next generation linear collider for a relative sneutrino mass-splitting of order $\mathcal{O}(0.001)$ and sneutrino width of order $\mathcal{O}(1$ GeV). On the other hand, the like sign dilepton event rate at the TEVATRON is probably too small to be observable.

1 Introduction

Recently there has been special interest in the bosonic counterpart of the neutrino appearing in supersymmetric (SUSY) extensions of the Standard Model [1], the sneutrino. This is due to the intimate relation of neutrino and sneutrino properties as regards the violation of the lepton number L: either both neutrino and sneutrino violate L or both do not [2, 3]. If L is violated, the sneutrino states in one generation exhibit a mass-splitting Δm=m_1-m_2, independent of the precise mechanism which generates L violation in the sneutrino sector. The masses $m_{1,2}$ correspond to the mass states $\tilde{\nu}_\ell^N$, N=1,2 (without mixing in generation space, ℓ denotes generation) which (in the effective low-energy theory) are the physical states instead of the weak interaction states $\tilde{\nu}_L(\ell), \tilde{\nu}_L^*(\ell)$ (degenerate in mass in the absence of L violation) [2, 3]. For the masses $m_{1,2}$ the relation $m_{1,2}$=$\overline{m}\pm\Delta m/2$ holds, where $\overline{m}$=$(m_1+m_2)/2$ is the average sneutrino mass.

Examples for the generation of a mass-splitting in the light sneutrino sector include the SUSY sea-saw mechanism [3] and bilinear R-parity violating models [4]. In the sea-saw picture, below the electroweak symmetry breaking scale L violation is transferred from $SU(2)_L$ singlet sneutrinos to the light sneutrino sector. In models with bilinear R-parity breaking $SU(2)_L$ doublet sneutrinos mix with the Higgs sector and automatically violate L.

The amount of L-violation (or equivalently Δm) is restricted by the kinematical upper limits on neutrino masses and neutrinoless double beta decay [5, 6]: the limit on Δm is very stringent for the first generation, but leaves room for appreciable L violation for the second and third generation (see the more detailed discussion in section 5). For example, the SUSY inverse of $0\nu\beta\beta$ could be observable at a future

muon collider [7]. If the electroweak phase transition is weakly first or second order, a generation independent constraint on the mass splitting is set by baryogenesis [8].

A mass splitting also implies that the lightest sneutrino state may become the lightest supersymmetric particle (LSP) and - if its mass is around 70 GeV - a candidate for the cold dark matter in the universe [9]. This case should be easily discernable at a future lepton collider facility [10]. In the absence of L violation the sneutrino cannot account for the cold dark matter in the universe [11, 12]. In collider experiments, L violation in the sneutrino sector could manifest itself by a wrong sign lepton stemming from the decay of a sneutrino in a lepton and a chargino [5, 3]: the electric charge of the lepton produced in the decay of sneutrinos (assumed heavier than charginos)

$$\tilde{\nu}_\ell^N \to \ell^\pm \chi^\mp \tag{1}$$

may be of the wrong sign compared to the L-conserving case. In sneutrino pair production or associated single sneutrino production mechanisms the signal final state then contains a pair of like sign leptons (like sign dilepton or LSD). In the following, the LSD will be used as a signal for sneutrino-induced L violation and its cross section at proton and electron colliders will be estimated for different sneutrino production mechanisms under the assumption that R-parity is conserved. The LSD in a R-parity violating scenario (without sneutrino L violation) has been considered in ref. [13]. In view of the constraints on the mass-splitting mentioned above the discussion will be focussed on L-violation in the second and third generation.

The most obvious channel for sneutrino production is pair production: $f\overline{f} \to \tilde{\nu}_\ell^1 \tilde{\nu}_\ell^2$ in the L-violating case or $f\overline{f} \to \tilde{\nu}_L(\ell)\tilde{\nu}_L^*(\ell)$ in the L-conserving case. Here f stands for either leptons or quarks. At the TEVATRON (LHC) the pair production cross section for a 100 GeV sneutrino is around 30 fb (200 fb) [14], but drops quickly for larger values of the sneutrino mass: for a 300 GeV sneutrino the cross section is 0.03 fb (3 fb).

On the other hand, at a future electron positron Linear Collider (LC) [15] or at an accompanying electron-photon collider [16] the available energy in the center of mass system (c.m.s.) may be substantially smaller than at the LHC and the sneutrino pair production may be not available. In this case single sneutrino production has to be considered in order to gain some insight into the sneutrino properties. Examples of processes, where a single sneutrino of any flavour is produced at the LC or an accompanying electron-photon collider are:

$$e^+e^- \to \tilde{\nu}_\ell^N \ell^\pm \chi_k^\mp \tag{2}$$

$$e^+\gamma \to \tilde{\nu}_\ell^N \overline{\nu}_\ell \tilde{\ell}^+ \tag{3}$$

$$e^+e^- \to \tilde{\nu}_\ell^N W^\pm \tilde{\ell}^\mp \ , \tag{4}$$

where k=1,2 and $\chi_2^\pm$ is the lighter of the two chargino states. In R-parity violating frameworks, in addition to the mechanisms Eqs. (1) single sneutrinos may be produced in resonances or in two body final states both at hadron or lepton colliders [13, 17].

The processes in Eqs. (2,3) can be regarded as the leptonic SUSY analogues of single top-quark production [18] in the SM. It should also be recalled that sneutrinos can in addition be produced with accompanying neutrinos and neutralinos, *e.g.* by the process $e^+e^- \to \tilde{\nu}_\ell^N \nu_\ell \chi_k^0$, resulting in a final state very difficult to observe or not observable at all. Hence this possibility will not be considered further.

As the aim of this work is largely exploratory the attention is focussed on the value of total cross sections which are estimated at the energies the TEVATRON, LHC and a future e^+e^- linear collider (LC). Kinematic cuts, which may be specific of the particular detector and/or experiment are not included. These can only

be implemented in a realistic MonteCarlo simulation of the signal with a parallel detailed study of the background which is however beyond the scope of this work. Nonetheless in order to have an idea of the observability of such phenomena the estimated total cross sections are compared to the (prospected) annual integrated luminosities of the TEVATRON, LHC and LC. The TEVATRON luminosity at $\sqrt{s}$=1.8 TeV is $\mathcal{L}_\circ$=$2fb^{-1}$, the LHC luminosity at $\sqrt{s}$=14 TeV is expected to be $\mathcal{L}_\circ$=$10fb^{-1}$-$100fb^{-1}$, and the projected luminosity of the TESLA LC project is [19] $L_\circ$=300 fb^{-1} at $\sqrt{s}$=500 GeV, and $L_\circ$=500 fb^{-1} at $\sqrt{s}$=800 GeV. It is also expected that the LC will be able to operate in the electron-photon ($e^-\gamma$), photon-photon ($\gamma\gamma$) and electron-electron (e^-e^-) modes with luminosities comparable to that of the underlying e^+e^- machine (even higher in the case of the $\gamma\gamma$ mode) [20].

The outline of this note is as follows: In the next section we start with an estimation of the LSD via sneutrino pair production at the TEVATRON, the LHC and the LC. In section 3 the LSD produced in the reaction of Eq. (2) is presented and in section 4 the LSD triggered by the process in Eq. (3) will be considered. Since the reaction in Eq. (4) produces a more difficult signature due to the additional W boson in the final state it will not be analysed. In section 5 the results are compared to low-energy constraints on Δm and section 6 contains the conclusions.

2 The LSD in sneutrino pair production at TEVATRON, LHC and LC

The graph contributing to the LSD generated by the Drell-Yan sneutrino pair production mechanism is depicted in Fig. 1 and its amplitude is given explicitely in appendix A, Eq. (23). The LSD is induced by the L-violating sneutrino propagator [2]

$$\langle 0|T[\tilde{\nu}(x)\tilde{\nu}(y)]|0\rangle = \int \frac{d^4k}{(2\pi)^4} e^{-ik(x-y)} \left[\frac{1}{m_1^2 - k^2 - im_1\Gamma_1} - \frac{1}{m_2^2 - k^2 - im_2\Gamma_2}\right] , \quad (5)$$

where Γ_N is the total width of sneutrino mass state N. In the small width approximation $1/(x^2+\epsilon^2) \approx \pi\delta(x)/\epsilon$ (for $\epsilon \ll x$) the LSD cross section becomes

$$\sigma^{LSD} = \sigma(\tilde{\nu}_1\tilde{\nu}_2)\ \xi^{pair}\ \frac{\Gamma_1(\chi^\pm l^\mp)}{\Gamma_1}\frac{\Gamma_2(\chi^\pm l^\mp)}{\Gamma_2} , \quad (6)$$

where $\Gamma_N(\chi^\pm l^\mp)$ is the partial width of sneutrino mass state N into chargino final states. The effect of L violation in sneutrino pair production is measured by the factor

$$\xi^{pair} = 1 - \frac{2m_1\Gamma_1 m_2\Gamma_2(m_1\Gamma_1 m_2\Gamma_2 + (\Delta m^2)^2)}{m_1^2\Gamma_1^2 m_2^2\Gamma_2^2 + [(\Delta m^2)^2 + m_1^2\Gamma_1^2]\,[(\Delta m^2)^2 + m_2^2\Gamma_2^2]} , 0 \le \xi < 1 . \quad (7)$$

The factor ξ^{pair} is plotted in Fig. 4 for two sets of sample parameters defined in Table 1 and for different values of $\overline{m}$ as a function of the relative mass-splitting

$$\mathcal{R} := \frac{\Delta m}{\overline{m}} \ : \quad (8)$$

ξ^{pair} is of order $\mathcal{O}(1)$ for $\mathcal{R} \sim \mathcal{O}(0.01)$ for moderate values of $\overline{m}$, whereas, for large $\overline{m}$, ξ^{pair} is of order $\mathcal{O}(1)$ only if $\mathcal{R}$ is of order $\mathcal{O}(0.1)$.

Integrating over the parton distribution functions, the cross section in Eq. (6) to be expected at the TEVATRON and at the LHC is plotted in Fig. 5 and Fig. 6. (our results for the bare pair production cross section coincide with the results of ref. [14]).

The total sneutrino width is estimated taking into account only two body decay modes

$$\tilde{\nu}_\ell^{1,2} \to \ell^\pm \chi_j^\mp \ , \ \tilde{\nu}_\ell^{1,2} \to \nu \chi_j^0. \tag{9}$$

since it is assumed that the sneutrino is heavier than the lighter chargino. For the parameters chosen in Table 1 the difference between the average sneutrino mass and the charged slepton mass is smaller than the mass of the weak gauge bosons. However, for a large mass-splitting the heavier sneutrino may decay as $\tilde{\nu}_\ell^1 \to \tilde{\ell}^\pm + W^\mp$. Since the charged slepton usually decays with a large branching fraction into a neutralino-lepton final state, the L-violating signal would be slightly enhanced.

The final state charginos decay themselves mainly into the LSP neutralino and a fermion pair (to a small fraction charginos decay into four-fermion final states via gluinos or non-LSP neutralinos, see the detailed discussion in ref. [23]). Therefore the signal final states are

$$\mathrm{LSD}^\pm + \ell^\mp + \ell^{`\mp} + \not{E} \,, \ \mathrm{LSD}^\pm + \ell^\mp + \ 2 \text{ jets } + \not{E} \,, \ \mathrm{LSD}^\pm + \ 4 \text{ jets } + \not{E} \,. \tag{10}$$

That is, if both charginos decay into leptons the final state may be an exotic "double" LSD, *e.g.* $\tau^-\tau^- e^+ \mu^+$. In the SM, a LSD is produced in the decays of $t\overline{t}$, $b\overline{b}$, WW, WZ and ZZ pairs or a singly produced t, *c.f.* the discussion in ref. [13]. The LSD in such events is, apart from a LSD in ZZ production, always accompanied by jets, therefore the purely leptonic final states in Eq. (10) remain unaffected by such a background. The background from the decays of ZZ pairs into four charged leptons of same generation is vetoed by requiring $\not{E} > 2m_{LSP}$.

As regards the semihadronic final states, provided that the velocity of the decaying sneutrinos is large enough, the background event topology differs from the signal topology: hadron pairs decay into an odd number of jets on each side, while the number of jets in hadronic chargino decays is even; the LSD in the decays of a WW pair is accompanied by four jets on one side, the LSD in a semihadronic decay of a ZZ pair contains four jets on one and two jets on the other side, and the LSD in the decay of WZ is accompanied by one single lepton.

Conceivable SUSY background stems from decaying squark or gaugino pairs (in analogy to the SM background mentioned above) and decaying slepton pairs. Here the LSD in decays of non-LSP neutralinos into two charged lepton pairs may be eliminated rejecting events containing four same-generation charged leptons. The LSD in the decay of a slepton pair is accompanied by a one-sided lepton pair in contrast to a single lepton in the signal final state. In respect to semi-hadronic LSD production channels, the same remarks as in the SM case apply. It therefore may be concluded that the signal is virtually background-free.

At the TEVATRON, even in favourable circumstances the LSD cross section (Eq. 6)for the parameter sets chosen is, at most, of order $\mathcal{O}(0.1$ fb), see Fig. 5. Note that for large values of $\mathcal{R}$ and small $\overline{m}$ the LSD cross section drops to zero since the lighter sneutrino cannot decay into the wrong sign charged lepton final state. Hence the resulting event rate at TEVATRON is less than one event per year and detecting a sneutrino-induced LSD seems to be virtually impossible.

Given the larger ***pp*** c.m.s. energy and luminosity the prospects of detecting a sneutrino-induced LSD certainly seem much brighter at the LHC. Since the LSD is virtually background-free, one LSD event per year could be sufficient for detecting the effect. This in turn implies that for a LHC-luminosity of $\mathcal{L}_\circ$=$10 fb^{-1}$ ($\mathcal{L}_\circ$=$100 fb^{-1}$) a cross-section of 0.1fb (0.01fb) yields an observable LSD signal. Therefore for $\overline{m}$ not much larger than 200 GeV the LSD is observable (for both projected luminosities) for $\mathcal{R}$ being of order $\mathcal{O}(10^{-3})$, see Fig. 6. Even for $\overline{m}$ as large as 600 GeV the LSD could be visible if $\mathcal{L}_\circ$=$100 fb^{-1}$ and $\mathcal{R}$ being of order $\mathcal{O}(0.01)$ (without L violation the LHC may search for sleptons not much larger than

350 GeV [14]). In section 5 the range of $\mathcal{R}$ yielding an observable LSD signal is compared with the limits on Δm from neutrino masses.

Finally, at a LC with a c.m.s. energy of 500 GeV (800 GeV) and for $\overline{m}$ not much larger than 220 GeV (300 GeV), the LSD cross section is of order $\mathcal{O}$(0.01 fb) (yielding an annual event rate of order $\mathcal{O}$(few/year)) for $\mathcal{R}$ of order $\mathcal{O}(10^{-3})$, see Fig. 7.

In section 5 the range of $\mathcal{R}$ yielding an observable LSD signal at the LHC and LC is compared with the limits on Δm from neutrino masses.

3 The LSD in the reaction $e^+e^- \to \chi^\pm \tilde{\nu}^N_\ell \ell^\mp,\ \ell = \mu, \tau$

The Feynman graphs contributing to this reaction are depicted in Fig. 2 if the flavour of the final state sneutrino is either ℓ=μ or ℓ=τ. If ℓ=e, then further contributions similar to those examined in [21] (replacing the proton with an electron) have to be taken into account. The resulting cross section can be written as

$$\sigma^{tot} = \sum_{k,l=\mathrm{I};k\leq l}^{\mathrm{III}} \sigma^{(k,l)} \tag{11}$$

where *e.g.* $\sigma^{\mathrm{I,II}}$ is the contribution from the interference of s-channel gauge boson exchange (Fig. 2-I) and t-channel sneutrino exchange (Fig. 2-II). The explicit expressions of the various contributions are listed in appendix B.

Since the graph in Fig. 2-III contains the derivative coupling of the Z^0 to the sneutrinos (see the previous section), its contribution is β-suppressed below the threshold of sneutrino pair production. For the sneutrino mass range considered in this section it is therefore always much smaller than the modes in Figs. 2-I and 2-II and in the following it is neglected.

The three-particle phase space integral of graphs can be split into two two-particle phase space integrals (see *e.g.* ref. [22]), so that the phase space integrals relative to the contributions in Fig. 2-I and 2-II (and their interference) can be evaluated analytically up to the integration over Q^2 to be integrated numerically, where Q is the sum of the lepton and sneutrino impulses. We have checked, that using the small width approximation the three body cross sections $\sigma^{(\mathrm{III,III})}$ and $\sigma^{(\mathrm{I,I})+(\mathrm{II,II})+(\mathrm{I,II})}$ simplify in factorised expressions of the sneutrino and chargino pair production times the corresponding sneutrino and chargino partial decay width if kinematically allowed.

If the final state sneutrino is lighter than at least one of the charginos, the cross section depends very sensitively on the chargino width. However, in what follows the sneutrino will taken to be heavier than both charginos and their width will be neglected. In Fig. 8 the cross section Eq. (11) is plotted for the L-conserving case in terms of the final state sneutrino mass for two sets of SUSY parameters $\mu, M_2, \tan\beta$ (μ is the Higgs mixing parameter, M_2 is the gaugino mass associated to $SU(2)_L$, and $\tan\beta$ is the ratio of the vacuum expectation values of the two Higgs doublets) defined in Table 1 and for beam energies $\sqrt{s}$=500 GeV and $\sqrt{s}$=800 GeV. In the following the unification condition in a minimal supergravity (mSUGRA) model M_1=(5/3)$M_2\times\tan^2\Theta_W$ is assumed unless stated otherwise. In the sneutrio mass region where sneutrino pair production is kinematically excluded the cross section is of order $\mathcal{O}$(0.1 fb) or less.

In order to estimate the cross section for the LSD, we use the L-violating propagator Eq. (5) and again apply the small width approximation. The cross section Eq. (11) becomes:

$$\sigma^{LSD} \;=\; \xi^{single}\left[\sigma^{tot}(\tilde{\nu}^1)\frac{\Gamma_1(\chi^\pm\ell^\mp)}{\Gamma_1}\Theta(m_1^2-\bar{s}_-)\Theta(\bar{s}_+-m_1^2)\,+\right.$$

$$\sigma^{tot}(\tilde{\nu}^2)\frac{\Gamma_2(\chi^{\pm}\ell^{\mp})}{\Gamma_2}\Theta(m_2^2-\bar{s}_-)\Theta(\bar{s}_+-m_2^2)\Big] \ , \qquad (12)$$

where

$$\bar{s}_+ = \sqrt{s} - m_{\chi_2} - m_\ell \ , \quad \bar{s}_- = m_{\chi_1} + m_\ell .$$

The definition of $\bar{s}_-$ implies that the light sneutrino state contributes only if it is heavier than both charginos. Otherwise the light sneutrino may be produced by the decays of a real chargino and the width has to be taken into account (see the comment above). The L-violating factor ξ^{single} measures the effect of L violation in single sneutrino production and is defined as

$$\xi^{single} = 1 - \frac{2m_1\Gamma_1 m_2\Gamma_2}{(\Delta m^2)^2 + m_1^2\Gamma_1^2 + m_2^2\Gamma_2^2} \ , \quad 0 \leq \xi < 1 \ . \qquad (13)$$

The behaviour of ξ^{single} in dependence on $\mathcal{R}$ is illustrated in Fig. 9. For the parameters chosen ξ^{single} is of order $\mathcal{O}(1)$ for $\mathcal{R}$ being of order $\mathcal{O}(0.1)$.

The LSD signal final states in single sneutrino production are the same as in pair production listed in Eq. (10), though the topology is different: the LSD lepton pair is one-sided, whereas in pair production it is back to back. Conceivable SM and SUSY background sources are the same as in sneutrino production, and in prinicple the same remarks concerning their suppression apply. However, the one-sidedness of the LSD in single sneutrino production is not inherent to any of the SM or SUSY background sources and itself provides a powerful criterium to distinct signal from background. Therefore again it seems reasonable to conclude that the signal is virtually background-free and we assume that an event rate of order $\mathcal{O}(1/\text{year})$ is sufficient to detect the effect so that for an integrated luminosity of order $\mathcal{O}(\text{few}\times 100$ fb$^{-1})$ a cross section as small as $\mathcal{O}(0.01$ fb) could be measured.

In Fig. 10 the cross section for the L-violating signal is plotted versus the relative sneutrino mass-splitting $\mathcal{R}$ for the parameter sets as defined in Table 1 and for different values of the average sneutrino mass $\overline{m}$. The dominant contribution comes always from the lighter sneutrino state, and in extending the amount of L-violation it has been made sure that the lighter sneutrino is sufficiently heavy so that the widths of both charginos may be safely neglected. In the cases ($\overline{m}$=275 GeV; $\sqrt{s}$=500 GeV; set A) and ($\overline{m}$=450 GeV; $\sqrt{s}$=800 GeV; sets A and B) a relative mass-splitting $\Delta m/\overline{m}$ of order $\mathcal{O}(0.01)$ is sufficient to produce an L-violating cross section of order $\mathcal{O}(0.01$ fb). For the remaining cases ($\overline{m}$=350 GeV; $\sqrt{s}$=500 GeV; set A) and ($\overline{m}$=600 GeV; $\sqrt{s}$=800 GeV; sets A and B) the relative mass-splitting has to be one or two orders of magnitude larger in order to produce a visible signal. The range of $\mathcal{R}$ yielding an observable LSD signal is compared to the low energy limits on Δm in section 5.

4 The LSD in the reaction $e^+\gamma \to \tilde{\nu}_\ell^N \tilde{\ell}^+ \overline{\nu}_e, \ , (\ell = \mu, \tau)$

In electron-photon collisions μ- and τ-sneutrinos are necessarily produced by graphs at least of order three in perturbation theory. The dominant contributions to higher generation sneutrino production at an electron-photon collider are the ones depicted in Fig. 3, which, as mentioned above, are the leptonic SUSY equivalents to single top-quark production in the SM at an electron-photon facility [18] (the conventions adopted in this section follow closely those of [18]). For the production of first generation slepton pairs additional contributions have to be taken into account, replacing for example in Fig. 3-III the W-boson by a chargino and interchange the sneutrino and the neutrino, and similarly for the remaining contributions. The

relevant SUSY interaction Lagrangian are [1]:

$$\begin{aligned}
\mathcal{L}_{W\tilde{\nu}\tilde{\ell}} &= \frac{-ig}{\sqrt{2}} W^+_\mu (\tilde{\nu}^*_{\ell,L} \overset{\leftrightarrow\mu}{\partial} \tilde{\ell}_L) + h.c. \ , \\
\mathcal{L}_{\gamma\tilde{\ell}\tilde{\ell}} &= ieA_\mu \ \tilde{\ell}^*_{L,R} \overset{\leftrightarrow\mu}{\partial} \tilde{\ell}_{L,R} \ , \\
\mathcal{L}_{\gamma W\tilde{\ell}\tilde{\nu}} &= \frac{g}{\sqrt{2}} eA^\mu \tilde{\ell}^*_L \tilde{\nu}_{\ell,L} W^+_\mu + h.c. \ .
\end{aligned} \tag{14}$$

The gauge invariant amplitude consists of four terms and can be written as

$$\mathcal{M} = \frac{ieg^2}{2} \sum_{i=\mathrm{I}}^{\mathrm{IV}} T^i_\mu \epsilon^\mu(p_g) \ . \tag{15}$$

The various contributions are listed in Appendix C.

Here it is not possible to factorize the phase space integral into two two-particle integrations as it was done in the previous section so that the phase space integration is performed numerically using the VEGAS [24] code. Following [25], in the frame $\vec{\mathbf{p}}_{\tilde{\nu}} = -\vec{\mathbf{p}}_{\tilde{\ell}}$ the total cross section is given by

$$\sigma_{tot}(s) = \frac{1}{1024\pi^4} \int\limits_{(m_{\tilde{\nu}^N_\ell}+m_{\tilde{\ell}})^2}^{s} ds_2 \int\limits_{-(s-s_2)}^{0} dt_1 \int d\cos\theta \, d\phi \frac{\lambda^{1/2}(s_2, m^2_{\tilde{\nu}^N_\ell}, m^2_{\tilde{\ell}})}{s_2} |\mathcal{M}|^2 \ , \tag{16}$$

where $s_2 = (p_{\tilde{\ell}} + p_{\tilde{\nu}^N_\ell})^2$ and $t_1 = (p_e - p_\nu)^2$. The explicit parameterization of the individual four-vectors in terms of the invariants s_2, t_1 and the polar angles of $\vec{\mathbf{p}}_{\tilde{\ell}}$ is given in appendix D.

However the $e\gamma$ option of a LC will be realized producing high energy photons through Compton-backscattering of a low energy laser beam with an high energy positron beam [16]. Thus the resulting photons are not monochromatic and one has to fold the cross section of any $e\gamma$ process over a photon energy spectrum. It is expected that a photon collider will operate at luminosities very close to that of the e^+e^- machine. In terms of the variables

$$x = \frac{4E_{e^+}E_{Laser}}{m^2_e} \leq 2(1+\sqrt{2}) \quad , \quad y = \frac{E_\gamma}{E_{e^+}}$$

the photon energy spectrum is given by [26]

$$\mathcal{P}(y) = \frac{1}{N}\Big[1 - y + \frac{1}{1-y} - \frac{4y}{x(1-y)} + \frac{4y^2}{x^2(1-y)^2}\Big] \ . \tag{17}$$

Here the factor

$$N = \frac{1}{2} + \frac{8}{1+x} + \frac{7}{2x(1+x)} + \frac{1}{2x(1+x)^2} + (1 - \frac{4}{x} - \frac{8}{x^2}) \ln(1+x)$$

normalizes $\int \mathcal{P}(y)dy$ to unity. The resulting cross section applying Eq. (17) is

$$\sigma = \int\limits_{(m_{\tilde{\nu}^N_\ell}+m_{\tilde{\ell}})^2/s}^{x(x+1)} \mathcal{P}(y) \ \sigma_{tot}(ys) \ dy \ . \tag{18}$$

where σ_{tot} is defined in Eq. (16). Assuming the mSUGRA relations for the slepton masses [27]

$$\begin{aligned} m^2_{\tilde{\nu}_L} &= M_0^2 + 0.07 m^2_{\tilde{g}} + \frac{1}{2}\cos 2\beta M_Z^2 \\ m^2_{\tilde{\ell}_L} &= M_0^2 + 0.07 m^2_{\tilde{g}} + \frac{1}{2}\cos 2\beta M_Z^2 (2\sin^2\Theta_W - 1) \end{aligned}$$

The cross section Eq. (16) is plotted in Fig. 11 for the parameters defined in Table 1 and for two different values of the center-of-mass energy of the e^+e^--pair (x was set to its maximum). The cross section is of order $\mathcal{O}(0.1$ fb) at $\sqrt{s}$=800 GeV and M_0 masses of order $\mathcal{O}(100$ GeV). For a more realistic center of mass energy of 500 GeV the resulting cross sections are about an order of magnitude smaller. With luminosities as those projected for a LC of several 10^{34} cm^{-2}s^{-1} one produces several tens of single sneutrino events per year.

The process $e^+\gamma \to \tilde{\nu}^N_\ell \tilde{\ell}^+ \overline{\nu}_e$, ($\ell = \mu, \tau$) can also be exploited at e^+e^- colliders. Here infact by taking the photon to be virtual the diagrams of Fig. 3 can be attached to the electron current thus describing slepton associated single sneutrino production at e^+e^- colliders The full process involving virtual photons (with possibly other diagrams) due to the fact that the photon is massless (its propagator gives a factor Q^{-4} in the squared amplitude if Q is the virtual photon momentum) is dominated by small values of Q i.e. quasi real photons and the full e^+e^- process is approximated by folding the cross section of Eq. (16) with a photon distribution function $f_\gamma(x)$. This is the so-called equivalent photon (Weiszäcker-Williams) approximation (E.P.A) which, quite generally, for any scattering process involving a charged particle in the initial state that interacts via a virtual photon, consist in approximating the full process by defining a distribution function for the photon in the electron of energy E. The Weiszäcker-Williams spectrum is given by [28]

$$f_\gamma(x) = \frac{\alpha}{\pi}\log\left(\frac{E}{m_e}\right)\frac{1+(1-x)^2}{x}$$

and $f_\gamma(x)$ is interpreted as the photon distribution of an electron of energy E i.e. the probability that an electron of energy E radiates a quasi-real photon in the forward direction with energy $E_\gamma = xE$. The cross section at the e^+e^- machine is estimated using the following formula:

$$\sigma = \int_{(m_{\tilde{\nu}^N_\ell}+m_{\tilde{\ell}})^2/s}^{1} f_\gamma(x)\ \sigma_{tot}(xs)\ dx\ . \tag{19}$$

Some examples of the results employing Eq. (19) for the production of second and third generation single sneutrinos are shown in Fig. 11. Again, for plausible values of slepton masses and center-of-mass energies the resulting total cross sections are of the order of $\mathcal{O}(0.1fb)$. Therefore, as in the production of first generation sneutrinos (see ref. [29]) the production of second and third generation sneutrinos at an e^+e^- collider through the $e\gamma$ subprocess appears to be at observable rates provided that the LC will operate at the prospected luminosities of several 10^{34} cm^{-2} s^{-1}.

Applying the procedure of the previous section, it is possible to estimate the rate of wrong charged lepton events coming from L-violating sneutrino decays. If the initial state lepton is a positron, the signal final states are (assuming the final state leptons being not too soft)

$$\mathrm{LSD}^+ + \chi^- + \not{E}\ \ (\text{for } \tilde{\ell}^+ \to \ell + \chi^0)\ , \tag{20}$$

$$\ell^+ + \chi^- + \chi^+ + \not{E}\ \ (\text{for } \tilde{\ell}^+ \to \chi^+ \overline{\nu}_\ell)\ , \tag{21}$$

and the possible chargino decay modes have been mentioned in section 2. In the SM the second or third generation LSD in Eq. (20) may be produced in e-γ-collisions in at least 7th order of perturbation theory in the decay chain of a top-bottom final state (with additional CKM suppression). The rate of such a process is negligible even compared to the very low signal rate. The wrong charged sign lepton in Eq. (21) may be mimicked by the production of a Z^0-e^+ pair (the Z^0 decaying into ℓ's), when the charginos to a large fraction decay into the $\ell^+\nu_\ell\chi^0$ final state. The same reasoning holds for the SUSY background: *e.g.* the final state containing two charginos may be reproduced by the decays of a selectron and a non-LSP neutralino

$$e^+\gamma \to \tilde{e}^+\chi^0 \ , \tilde{e}^+ \to \chi^+\overline{\nu}_e \ , \chi^0 \to \chi^-\ell^+\nu_\ell \ .$$

If the $\tilde{\ell}$ decays to a large fraction directly into the LSP (thus producing a $\ell^+\ell^+$ final state) the background may be eliminated discarding events with only one ℓ^+ in the final state. In the opposite case, a detailed analysis of the angular and energy distribution of the final state particles is required.

The resulting cross section for the LSD signal and the wrong sign charged lepton signal is plotted in Fig. 12 for different combinations of parameters. In the examples chosen, for a moderate ratio $\mathcal{R} \sim 10^{-2}$ the L-violating signal may be observable only if both sleptons and charginos are light ($M_0 \approx M_2 \approx |\mu| \approx 100$ GeV). For higher masses an appreciable signal is reached only for a large amount of L-violation.

Note that in mSUGRA the $SU(2)_L$-doublet charged sleptons are slightly heavier than the $SU(2)_L$-doublet sneutrinos. This fact renders the process discussed here less favourable than the process discussed in the previous section. Larger cross sections for single μ- and τ-sneutrino production may be possible in scenarios where charged sleptons are allowed to be (considerably) lighter than the sneutrinos. Two examples shown in Fig. 13 illustrate this fact. For the parameters chosen, L-violating cross sections of order $\mathcal{O}(0.01$ fb) can be obtained for $\mathcal{R} \sim 0.01$ for higher values of $\overline{m}$ in respect to the mSUGRA case in Fig. 12. In the next section the range of $\mathcal{R}$ rendering an observable L-violating signal is compared to the low-energy constraints on Δm.

5 Observability of the LSD SIGNAL in view of low–energy constraints on Δm

The results for the LSD signal obtained in the previous sections should be compared to the low-energy limits on the sneutrino mass-splitting. The most stringent bounds on Δm come from the smallness of neutrino masses: loops containing L-violating sneutrinos and neutralinos contribute to the Majorana neutrino mass matrix $\mathcal{M}_{LL}$ mixing the $SU(2)_L$ doublet fields [5, 6, 3]. In ref. [6] a scan over a large range of the SUSY parameter space has been carried out and the following "absolute" limit has been derived from the upper limits on neutrino masses:

$$\Delta m(\ell) < 156 \, \frac{m_\nu^{exp}(\ell)}{1 \text{ eV}} \text{ keV} \ , \tag{22}$$

where $\overline{m}$ has been set to 100 GeV. Higher values for $\overline{m}$ result in less stringent bounds. This in turn implies that: (i) a relative mass-splitting $\mathcal{R} \sim 10^{-2}$ (yielding observable LSD event rates in sneutrino pair production at the LHC and a LC and in single sneutrino production at a LC) is compatible with a neutrino mass of order $\mathcal{O}(10$keV) and (ii) $\mathcal{R}$ being of order $\mathcal{O}(10^{-3})$ (yielding observable LSD event rates in sneutrino pair production at the LHC and a LC) is compatible with a neutrino mass of order $\mathcal{O}(1$ keV). It is interesting to note that a neutrino with a mass of order

$\mathcal{O}(1$ keV) could provide warm dark matter without overclosing the universe [30]. The current kinematical limits on neutrino masses are [31]

$$m_\nu^{exp}(e) < 3 \text{ eV} \ , \ m_\nu^{exp}(\mu) < 190 \text{ keV} \ , \ m_\nu^{exp}(\tau) < 18.2 \text{ MeV} \ ,$$

i.e. the kinematical limits leave room for an observable sneutrino mass-splitting in LSD events in the second and third generation.

On the other hand, the limit on the m_{ee} entry of $\mathcal{M}_{LL}$ from the Heidelberg-Moscow $0\nu\beta\beta$-decay experiment [32] together with the preliminary results of neutrino oscillation experiments (for a recent overview see *e.g.* [33]) imply that all entries of $\mathcal{M}_{LL}$ should satisfy $m_{ij} \lesssim 2.5$ eV [34]. If the oscillation solution (requiring mass-squared differences between the neutrino states of order $\mathcal{O}(1 \text{ eV}^2)$ or less) will be confirmed both for the atmospheric and for the solar neutrino problem, sneutrino-induced L violation will not be directly visible for sneutrino decay widths of order $\mathcal{O}(1$ GeV). If, on the other hand, the oscillation solution to one or both of the neutrino problems are not confirmed, several entries of $\mathcal{M}_{LL}$ are no longer required to be small, and neutrinos could still be much heavier than currently accepted.

Furthermore, it has been pointed out in ref. [3] that sneutrino oscillations could be observable even for neutrino masses of order $\mathcal{O}(1$ eV) provided that the total decay widths of the sneutrino mass states are very small. In the approach taken here this means that ξ is of order $\mathcal{O}(1)$ for very small values of Δm. As an example, this fact is illustrated for associated sneutrino production at a future LC: for a neutrino mass of 1 eV (corresponding to Δm=156 keV) the L-violating cross section for set A and $\sqrt{s}$=500 GeV is of order $\mathcal{O}(0.01$ fb) provided that the sneutrino widths are of order $\mathcal{O}(1$ MeV), see Fig. 14 where the sneutrino width has been varied freely. Such tiny sneutrino widths are conceivable for a small mass difference of sneutrinos in respect to the lighter chargino and the LSP neutralino (still it has to made sure that the final state leptons are not too soft to be detectable). This is usually impossible in a mSUGRA context, where the LSP is considerably lighter than the lighter chargino, but in a more general context may well be possible. If *e.g.* $M_1 = M_2$, it is always possible to find regions in the SUSY parameter space where the sneutrino width becomes very small and L violation may be directly visible.

6 Conclusions

In conclusion, L violation in the sneutrino sector of supersymmetric extensions of the Standard Model may manifest itself by decays of sneutrinos into final states containing a like sign dilepton. Since the LSD signal is virtually background-free even very small event rates of order $\mathcal{O}(1/$year) could be observable at hadron, electron or electron-photon collider facilities.

At the LHC or a future electron linear collider (LC) with a c.m.s. energy of 800 GeV, an observable LSD is triggered in sneutrino pair production for a relative mass-splitting $\mathcal{R}$ being of order $\mathcal{O}(10^{-3})$ if the average mass of the two sneutrino mass states $\overline{m}$ is not much larger than 400 GeV. At a LC with a c.m.s. energy of 500 GeV the LSD is observable for $\mathcal{R}$ being of order $\mathcal{O}(10^{-3})$ if $\overline{m} \lesssim 220$ GeV. At the TEVATRON, the LSD event rate is less than one per year for realistic SUSY parameters and therefore virtually not observable.

If $\overline{m}$ is larger than the c.m.s. energy available (*e.g.* at 500 GeV next linear collider), sneutrino pair production is excluded and associated single sneutrino production has to be considered in future collider facilities such as a LC or an electron-photon machine. For chargino-associated single sneutrino prodution at a LC, under favourable cirumstances (large branching fraction of the chargino-lepton decay channel and a relative low average sneutrino mass) one may expect about

ten LSD events per year for $\mathcal{R}$ being of order $\mathcal{O}(0.01)$. Under unfavourable circumstances less than one LSD event per year is expected. Then an appreciable event rate is possible only for $\mathcal{R}$ being of order $\mathcal{O}(1)$.

For charged slepton associated sneutrino production at an electron-photon collider, in mSUGRA models the event rate of the LSD or the wrong charged lepton signal is very low for realistic slepton masses and $\mathcal{R}$ being of order $\mathcal{O}(0.01)$. In order to produce a detectable event rate $\mathcal{R}$ must be close to one. If the charged slepton is considerably lighter than the average sneutrino mass, an observable event rate is possible for moderate values of the mass-splitting.

L violation in the sneutrino sector induces radiative contributions to the left-handed Majorana mass-matrix $\mathcal{M}_{LL}$: $\mathcal{R}$ being of order $\mathcal{O}(10^{-3})$ corresponds to a neutrino mass of order $\mathcal{O}(1$ keV), $\mathcal{R}$ being of order $\mathcal{O}(10^{-2})$ corresponds to a neutrino mass of order $\mathcal{O}(10$ keV). Such an amount of L violation is compatible with the kinematical limits on second and third generation neutrino, but not compatible with the limits on the entries of $\mathcal{M}_{LL}$ from the neutrinoless double beta decay combined with the oscillation solution to the solar and atmospheric neutrino problems.

Acknowledgments

O. P. would like to thank the Max-Plank-Institut für Kernphysik, for the very warm hospitality during his stay in Heidelberg. The work of St. K. was in part supported by a Marie Curie Individual Fellowship (European Union), under contract N. HPMF-CT-2000-00752.

A LSD in sneutrino pair production

The amplitude for the LSD in sneutrino pair production at a hadron collider is (see Fig. 1)

$$\begin{aligned} \mathcal{T}_{fi} &= \frac{g^4}{4\cos^3\Theta_W} V_{i1}V_{i'1}|\mathcal{D}_Z(s)|^2(p_{34}-p_{12})\cdot j^{quark}j^{lep}_{il}j^{lep}_{i'l'} \\ &\times \left(\mathcal{D}_1(s_{34})\mathcal{D}_2(s_{12})-\mathcal{D}_1(s_{12})\mathcal{D}_2(s_{34})\right) . \end{aligned} \tag{23}$$

Here j are the quark and lepton currents and propagator factors are denoted as $\mathcal{D}(x)=(m^2-x-i\Gamma m)^{-1}$. The invariants are $s_{12}=p_{12}^2=(p_i+p_l)^2$, $s_{34}=p_{34}^2=(p_i'+p_l')^2$ an V is the chargino mixing matrix. Note that Eq. (23) reflects the off-diagonality of the sneutrino-Z vertex.

B Contributions to $e^+e^- \to \chi^\pm\tilde{\nu}_\ell^N\ell^\mp$, $\ell=\mu,\tau$

In the following individual contributions to the cross section for the reaction $e^+e^- \to \chi^\pm\tilde{\nu}_\ell^N\ell^\mp$ (Fig. 2) are listed for $\ell=\mu,\tau$. For $\ell=e$ further contributions have to be taken into account. The contribution of the Higgs exchange diagram has been neglected since it is proportional to the electron mass. The index i corresponds to the final state chargino (for obtaining numerical results only production of the lighter chargino was considered), the indices j,j' correspond to exchanged charginos. V,V' stands for either γ or Z^0 and N is the index for the heavier (N=1) or lighter (N=2) sneutrino mass states. m_D is the usual L-conserving sneutrino mass. The modification of the sneutrino propagator in the presence of L violation has been neglected. Propagator factors $1/\left[(M^2-X)^2+M^2\Gamma_M^2\right]$ are denoted by $P(M,X)$. The integration limits of $Q^2=(p_{m_{\tilde{\nu}_\ell^N}}+p_\ell)^2$ are

$$Q^2_{max,min}=(\sqrt{s}-m_i)^2,(m_\ell+m_{\tilde{\nu}_\ell^N})^2$$

unless noted otherwise. The total cross section is a sum of the contributions depicted in Fig. 2 and their interferences. The interference between 2-III and the other graphs is neglected since in the numerical examples displayed in Table 1 the contribution of 2-III is much smaller than the contribution from both 2-I and 2-II.

The contribution from (t-channel) sneutrino-exchange shown in Fig. 2-I is defined as

$$\begin{aligned}
\sigma_i^{(\mathrm{I,I})} &= \frac{1}{2s}\frac{1}{4}\sum_{j,j'} g^6 |V_i|^2 |V_j|^2 |V_{j'}|^2 \frac{1}{128\pi^3}\int dQ^2\ \lambda^{1/2}(1,\frac{m_\ell^2}{Q^2},\frac{m_{\tilde{\nu}_\ell^N}}{Q^2}) P(m_j,Q^2) \\
&\times \quad P(m_{j'},Q^2)(Q^2+m_\ell^2-m_{\tilde{\nu}_\ell^N}^2)((m_j^2-Q^2)(m_{j'}^2-Q^2)+m_j m_{j'}\Gamma_j\Gamma_{j'}) \\
&\times \quad \Big[\lambda^{1/2}(\frac{Q^2}{s},\frac{m_i^2}{s},1)(1+\frac{(Q^2-m_{\tilde{\nu}_\ell^N}^2)(m_i^2-m_{\tilde{\nu}_\ell^N}^2)}{(Q^2-m_{\tilde{\nu}_\ell^N}^2)(m_i^2-m_{\tilde{\nu}_\ell^N}^2)+m_{\tilde{\nu}_\ell^N}^2 s}) \\
&+ \quad \frac{1}{s}(2m_{\tilde{\nu}_\ell^N}^2-m_i^2-Q^2)\ln F(Q^2)\Big]\ ,
\end{aligned}$$

where as usual $\lambda(a,b,c)$=$a^2+b^2+c^2+2ab+2ac+2bc$ and the function $F(Q^2)$ is defined as

$$\begin{aligned}
F(Q^2) &= (m_i^2-\tilde{m}_D^2+\frac{1}{2}(Q^2-m_i^2-s)+\frac{1}{2}\lambda^{1/2}(Q^2,m_i^2,s)) \\
&\times \quad (m_i^2-\tilde{m}_D^2+\frac{1}{2}(Q^2-m_i^2-s)-\frac{1}{2}\lambda^{1/2}(Q^2,m_i^2,s))^{-1}\ .
\end{aligned}$$

The contribution from (s-channel) gauge-boson-exchange depicted in Fig. 2-II is defined as

$$\begin{aligned}
\sigma_i^{(\mathrm{II,II})} &= \frac{1}{2s}\frac{1}{4}\sum_{j,j'}\sum_{V,V'} g^2 V_{j1}V_{j'1}(g_V^L g_{V'}^L+g_V^R g_{V'}^R)\frac{1}{32\pi^3}\int dQ^2\ \lambda^{1/2}(1,\frac{m_\ell^2}{Q^2},\frac{m_{\tilde{\nu}_\ell^N}^2}{Q^2}) \\
&\times \quad (Q^2+m_\ell^2-m_{\tilde{\nu}_\ell^N}^2)\lambda^{1/2}(1,\frac{m_l^2}{s},\frac{Q^2}{s})P(V,s)P(V',s)P(j,Q^2)P(j',Q^2) \\
&\times \quad G(Q^2)\Big\{\frac{1}{3}s^2\Big[\lambda(1,\frac{m_i^2}{s},\frac{Q^2}{s})+(1+\frac{m_i^2}{s}+\frac{Q^2}{s}-\frac{2(m_i^2-Q^2)^2}{s^2})\Big] \\
&\times \quad \Big[Q^2(O'^L_{ji})_V(O'^L_{j'i})^*+m_j m_{j'}(O'^R_{ji})_V(O'^R_{j'i})^*_{V'}\Big] \\
&+ \quad 2Q^2 s\Big[m_{j'}m_i(O'^L_{ji})_V(O'^R_{j'i})^*_{V'}+m_{j'}m_i(O'^R_{ji})_V(O'^L_{j'i})^*_{V'}\Big]\Big\}\ ,
\end{aligned}$$

where the function $G(Q^2)$ is given by

$$\begin{aligned}
G(Q^2) &= \Big[(m_V^2-s)\{(m_{V'}^2-s)a-m_{V'}\Gamma_{V'}b\} \\
&+ \quad m_V\Gamma_V\{m_{V'}\Gamma_{V'}a+(m_{V'}^2-s)b\}\Big]\ ; \\
a &= (m_j^2-Q^2)(m_{j'}^2-Q^2)+m_j m_{j'}\Gamma_j\Gamma_{j'} \\
b &= m_{j'}\Gamma_{j'}(m_j^2-Q^2)-m_j\Gamma_j(m_{j'}^2-Q^2)\ .
\end{aligned}$$

The lepton-gauge boson couplings $g_V^{L,R}$ are

$$\begin{aligned}
g_{Z^0}^L &= \frac{g}{\cos\Theta_W}(\frac{1}{2}-\sin^2\Theta_W)\ \ ,\ \ g_{Z^0}^R=\frac{g}{\cos\Theta_W}(-\sin^2\Theta_W) \\
g_\gamma^L &= g_\gamma^R = e\ \ ,
\end{aligned}$$

and the gauge boson-chargino couplings $(O'^{L,R}_{ij})_V$ are

$$
\begin{aligned}
(O'^{L}_{ij})_{Z^0} &= \frac{g}{\cos\Theta_W}(-V_{i1}V^*_{j1} - \frac{1}{2}V_{i2}V^*_{j2} + \delta_{ij}\sin^2\Theta_W) \\
(O'^{R}_{ij})_{Z^0} &= \frac{g}{\cos\Theta_W}(-U^*_{i1}U_{j1} - \frac{1}{2}U^*_{i2}U_{j2} + \delta_{ij}\sin^2\Theta_W) \\
(O'^{L}_{ij})_{\gamma} &= (O'^{R}_{ij})_{\gamma} \;=\; -e\delta_{ij}
\end{aligned}
$$

(Note that $(O'^{L,R}_{ij})_V = (O'^{L,R}_{ji})^*_V$).

The interference between sneutrino and gauge boson graphs is

$$
\begin{aligned}
\sigma_i^{(\mathrm{I,II})} &= \frac{1}{2s}\frac{1}{4}\sum_{j,j'} g^4|V_{i1}|^2|V_{j1}|^2\frac{1}{32\pi^3}\int dQ^2\;(Q^2+m_l^2-m^2_{\tilde\nu^N_\ell})\lambda^{1/2}\Big(1,\frac{m_\ell^2}{s},\frac{Q^2}{s}\Big) \\
&\times\; P(j,Q^2)P(j',Q^2)P(V,s)\Big\{(m_V^2-s)\Big[(m_j^2-Q^2)(m_{j'}^2-Q^2)+m_j m_{j'}\Gamma_j\Gamma_{j'}\Big] \\
&-\; m_V\Gamma_V\Big[(m_j^2-Q^2)m_{j'}\Gamma_{j'}-(m_{j'}^2-Q^2)m_j\Gamma_j\Big]\Big\} \\
&\times\; \Big\{m_i m_{j'}(O'^{R}_{ij'})^*_V(-\ln F(Q^2)) + \frac{1}{2}(O'^{L}_{ij'})^*_V\Big[\lambda^{1/2}\Big(\frac{Q^2}{s},\frac{m_i^2}{s},1\Big) \\
&\times\; (\frac{1}{2}(Q^2+m_i^2-s)-\tilde m_D^2) - \frac{1}{s}(Q^2-\tilde m_D^2)(m_i^2-\tilde m_D^2)\ln F(Q^2)\Big]\Big\}
\end{aligned}
$$

and the function $F(Q^2)$ has been defined above.

The contribution from the double sneutrino graph is

$$
\begin{aligned}
\sigma_i^{(\mathrm{III,III})} &= \frac{1}{2s}\frac{1}{4}\frac{1}{(2\pi)^5}\frac{1}{8}|V_{i1}|^2\frac{g^6}{c_W^2}\frac{\pi^2}{3}s^2\int dQ^2\;P(m_{Z^0},s)P(m_{\tilde\nu_l^{N'}},Q^2) \\
&\times\; \lambda^{1/2}\Big(1,\frac{Q^2}{s},\frac{m^2_{\tilde\nu^N_\ell}}{s}\Big)\lambda^{1/2}\Big(1,\frac{m_\ell^2}{Q^2},\frac{m^2_{\chi_i}}{Q^2}\Big)(Q^2-m^2_{\chi_i}-m_\ell^2) \\
&\times\; \Big[1-2\frac{m^2_{\tilde\nu^N_\ell}}{s}-2\frac{Q^2}{s}-\frac{1}{2}\lambda\Big(1,\frac{Q^2}{s},\frac{m^2_{\tilde\nu^N_\ell}}{s}\Big)+\frac{(m^2_{\tilde\nu^N_\ell}-Q^2)^2}{s^2}\Big]\,.
\end{aligned}
$$

The integration limits are $Q^2_{min} = (m_\ell + m_{\chi_i})^2$ and $Q^2_{max} = (\sqrt{s} - m_{\tilde\nu^N_\ell})^2$. Note that $N \neq N'$ due to the off-diagonality of the $Z^0\tilde\nu^1_\ell\tilde\nu^2_\ell$ vertex.

C Contributions to $e^+\gamma \to \tilde\nu^N_\ell \tilde\ell^+ \overline{\nu}_e$, $\ell = \mu, \tau$

The indivual amplitudes of the graphs shown in Fig. 3 are given by

$$
\begin{aligned}
T^{(I)}_\mu &= -D(s_2)D(t_1)j^\alpha(p_-)_\beta(g^{\beta\nu}-\frac{Q^\beta Q^\nu}{m_W^2})S_{\mu\nu\alpha}\;, \\
T^{(II)}_\mu &= D(s_2)(p_-)_\alpha(g^{\alpha\nu}-\frac{Q^\alpha Q^\nu}{m_W^2})\overline{v}(p_e)\gamma_\mu\frac{-(\not p_g+\not p_e)}{s}\gamma_\nu P_L v(p_\nu)\;, \\
T^{(III)}_\mu &= -D(t_1)j_\mu\;, \\
T^{(IV)}_\mu &= D(t_1)\frac{1}{m_{\tilde l}^2-K^2}j^\alpha[K_\mu K_\alpha + (p_{\tilde\nu_l^N})_\alpha(K-p_{\tilde l})_\mu - (p_{\tilde l})_\mu K_\alpha]\;.
\end{aligned}
$$

The sum of the first and the third contribution can be simplified to give

$$
\begin{aligned}
(T^{(I)}+T^{(III)})_\mu &= D(s_2)D(t_1)j^\alpha p_-^\beta 2(g_{\alpha\beta}P_\mu + g_{\mu\alpha}(p_g)_\beta - g_{\mu\beta}(p_g)_\alpha) \\
&+\; D(s_2)\frac{-1}{s}p_-^\alpha\overline{v}(p_e)\gamma_\mu(\not p_g+\not p_e)\gamma_\alpha P_L v(p_\nu)\;.
\end{aligned}
$$

Here we have defined

$$p_- = p_{\tilde{l}} - p_{\tilde{\nu}_l^N},\ K = p_g - p_{\tilde{l}},\ Q = p_{\tilde{l}} + p_{\tilde{\nu}_l^N},\ P = p_e - p_\nu,\ t_1 = P^2,\ s_2 = Q^2,$$

$$j^\alpha = \overline{v}(p_e)\gamma^\alpha P_L v(p_{\overline{\nu}}),\ S_{\mu\nu\alpha} = -g_{\alpha\nu}(P+Q)_\mu + g_{\mu\alpha}(P-p_g)_\nu + g_{\mu\nu}(Q+p_g)_\alpha,$$

$$D(s_2) = (m_W^2 - s_2 + i\Gamma_W m_W)^{-1},\ D(t_1) = (m_W^2 - t_1)^{-1}\ .$$

Replacing in [18] the quark charges e_t, e_b by 0, 1 respectively and the quark current J^μ_{quark} by $p^\mu_- = p_{\tilde{\ell}} - p_{\tilde{\nu}_\ell^N}$ (stemming from the derivative $W\tilde{\ell}\tilde{\nu}_\ell$ coupling) leads to the equivalent expressions of the amplitudes $T_\lambda^{(\mathrm{III})}, T_\lambda^{(\mathrm{IV})}$ in [18]. A subtlety known from scalar electrodynamics arises in the calculation of the time ordered product of the propagators of the exchanged scalar fields. Here the additional contribution from taking the partial derivatives out of the time ordered product is cancelled by the $W\gamma\tilde{\nu}_\ell\tilde{\ell}$ four point vertex.

D Four-vector parametrization in terms of two invariants and two angles

In order to carry out the numerical phase space integration in the process $e\gamma \to \tilde{\ell}^+\tilde{\nu}_\ell^N\overline{\nu}_e$ following [25] the four-vectors in the process can be parametrized in terms of two invariants (see appendix C) and one solid angle as

$$p_\gamma = \begin{pmatrix} \frac{s-s_2}{2\sqrt{s_2}}\Big[\sin^2\Theta + (\cos\Theta + \frac{s_2-t_1}{s-s_2})^2\Big]^{1/2} \\ \sin\Theta\frac{s-s_2}{2\sqrt{s_2}} \\ 0 \\ \frac{s-s_2}{2\sqrt{s_2}}\Big[\cos\Theta\frac{s_2-t_1}{s-s_2}\Big] \end{pmatrix}\ ,\quad p_e = \begin{pmatrix} \frac{s_2-t_1}{2\sqrt{s}} \\ 0 \\ 0 \\ \frac{s_2-t_1}{2\sqrt{s}} \end{pmatrix}\ ,$$

$$p_\nu = \begin{pmatrix} \frac{s-s_2}{2\sqrt{s_2}} \\ \sin\Theta\frac{s-s_2}{2\sqrt{s_2}} \\ 0 \\ \cos\Theta\frac{s-s_2}{2\sqrt{s_2}} \end{pmatrix}\ ,\quad p_{\tilde{\ell}} = \begin{pmatrix} \Big[m_{\tilde{\ell}}^2 + \frac{\lambda(s_2, m^2_{\tilde{\nu}_\ell^N}, m^2_{\tilde{\ell}})}{4s_2}\Big]^{1/2} \\ \frac{\lambda(s_2, m^2_{\tilde{\nu}_\ell^N}, m^2_{\tilde{\ell}})^{1/2}}{2\sqrt{s_2}}\sin\theta\cos\phi \\ \frac{\lambda(s_2, m^2_{\tilde{\nu}_\ell^N}, m^2_{\tilde{\ell}})^{1/2}}{2\sqrt{s_2}}\sin\theta\sin\phi \\ \frac{\lambda(s_2, m^2_{\tilde{\nu}_\ell^N}, m^2_{\tilde{\ell}})^{1/2}}{2\sqrt{s_2}}\cos\theta \end{pmatrix}$$

$$p_{\tilde{\nu}_\ell^N} = \begin{pmatrix} \Big[m^2_{\tilde{\nu}_\ell^N} + \frac{\lambda(s_2, m^2_{\tilde{\nu}_\ell^N}, m^2_{\tilde{\ell}})}{4s_2}\Big]^{1/2} \\ -\vec{\mathbf{p}}_3 \end{pmatrix}\ ,$$

$$\cos\Theta = \frac{(s-s_2)(s_2-t_1) - 2s_2(s-s_2-t_1)}{(s_2-t_1)(s-s_2)}\ .$$

References

[1] H.E. Haber and G.L. Kane, Phys. Rep. 117 (1985) 76.

[2] M. Hirsch, H.V. Klapdor-Kleingrothaus and S. Kovalenko, Phys. Lett. B 398 (1997) 311.

[3] Y. Grossmann and H.E. Haber, Phys. Rev. Lett. 78 (1997) 3438.

[4] Y. Grossman and H.E. Haber, Phys. Rev. D 59 (1999) 093008.

[5] M. Hirsch, H.V. Klapdor-Kleingrothaus and S. Kovalenko, Phys. Lett. B 403 (1997) 291.

[6] M. Hirsch, H.V. Klapdor-Kleingrothaus and S. Kovalenko, Phys. Rev. D 57 (1998) 1947.

[7] M. Hirsch, H.V. Klapdor-Kleingrothaus, St. Kolb and S. Kovalenko, Phys. Rev D 57 (1998) 2020.

[8] H.V. Klapdor-Kleingrothaus, St. Kolb and V.A. Kuzmin, Phys. Rev. D 62 (2000) 035014.

[9] L.J. Hall, T. Moroi and H. Murayama, Phys. Lett. B 424 (1998) 305.

[10] St. Kolb, M. Hirsch, H.V. Klapdor-Kleingrothaus and O. Panella, Phys. Lett. B 478 (2000) 262.

[11] L.E. Ibáñez, Phys. Lett. B 137 (1984) 160; J.S. Hagelin, G.L. Kane and S. Raby, Nucl. Phys. B 241 (1984) 638.

[12] T. Falk, K.A. Olive and M. Srednicki Phys. Lett. B 339 (1994) 248.

[13] H. Dreiner, P. Richardson and M.H. Seymour, Phys. Rev. D 63 (2001) 055008.

[14] H. Baer, C. Chen and F. Paige, Phys. Rev. D 49 (1994) 3283; F. del Aguila and L. Ameteller, Phys. Lett. B 261 (1991) 326.

[15] H. Murayama and M.E. Peskin, Ann. Rev. Nucl. Part. Sci. 46 (1996) 533.

[16] I. Ginzburg, G. Kotin, V. Serbo and V. Telnov, Nucl. Instrum. and Meth. 205 (1983) 47; I. Ginzburg, G. Kotin, S. Panfil, V. Serbo and V. Telnov, Nucl. Instrum. and Meth. 219 (1984) 5.

[17] M. Chembtob and G. Moreau, Phys. Rev. D 59 (1999) 055003; J. Kalinowski, R. Rückl, H. Spiesberger and P.M. Zerwas, Phys. Lett. B 414 (1997) 297.

[18] O. Panella, G. Pancheri and Y.N. Srivastava, Phys. Lett. B 318 (1993) 241.

[19] A. Wagner, Nucl. Phys. B (Proc. Suppl.) 79, (1999) 643-651. Cern Courier, 40 2000, No.5, 19-20.

[20] V. Telnov, Int. J. Mod. Phys. A 15, 2577-2586 (2000).

[21] T. Wöhrmann and H. Fraas, Phys. Rev. D 52 (1995) 78.

[22] V. Barger and R. Phillips, "Collider Physics" (Addison-Wesley, Redwood City, CA, 1987).

[23] A. Bartl, H. Fraas and W. Majoretto, Z. Phys. C 30 (1986) 441.

[24] G. P. Lepage, J. Comput. Phys. 27, 192 (1978).

[25] E. Byckling and K. Kajantie, "Particle Kinematics" (John Wiley, 1973).

[26] A. Ghosal, A. Kundu and B. Mukhopadhyaya, Phys. Rev. D 57 (1998) 1972.

[27] J. Ellis, G.L. Fogli and E. Lisi, Nucl. Phys. B 393 (1993) 3.

[28] E. Fermi, Z. Phys. 29 (1924) 315; C. Weiszäcker and E. Williams, Z. Phys. 88 (1934) 612; H. Terazawa, Rev. Mod. Phys. 45 (1973) 615; P. Kessler, Acta Physica Austriaca, 41 (1975) 141-188.

[29] S. Hesselbach and H. Fraas, Phys. Rev. D 55 (1997) 1343.

[30] G.F. Giudice *et al.*, hep-ph/0012317.

[31] D.E. Groom *et al.*, Europ. Phys. J. C 15 (2000) 1.

[32] L. Baudis *et al.*, Phys. Rev. Lett. 83 (1999) 41.

[33] See talks at Neutrino 2000,
http://ALUMNI.LAURENTIAN.CA/www/physics/nu2000/

[34] G. Bhattacharyya, H.V. Klapdor-Kleingrothaus and H. Päs, Phys. Lett. B 463 (1999) 77.

Table 1: Parameters used for numerical results assuming a gravity mediated GUT scheme. V (N) is the chargino (neutralino) mixing matrix.

Set A: $\mu = -100$ GeV , $M_2 = 100$ GeV , $\tan\beta = 2$			
$m_{\chi_1^+} = 151.1$ GeV	$m_{\chi_2^+} = 100.3$ GeV	$V(1,1) = 0.89$	$V(1,2) = -0.44$
$m_{\chi_1^0} = 143.6$ GeV	$m_{\chi_2^0} = 134.5$ GeV	$m_{\chi_3^0} = 86.2$ GeV	$m_{\chi_4^0} = 54.8$ GeV
$N(1,1) = -0.20$	$N(2,1) = -0.21$	$N(3,1) = -0.11$	$N(4,1) = -0.95$
$N(1,2) = 0.78$	$N(2,2) = 0.30$	$N(3,2) = -0.51$	$N(4,2) = -0.18$
Set B: $\mu = -200$ GeV , $M_2 = 200$ GeV , $\tan\beta = 35$			
$m_{\chi_1^+} = 263.5$ GeV	$m_{\chi_2^+} = 153.2$ GeV	$V(1,1) = 0.80$	$V(1,2) = -0.60$
$m_{\chi_1^0} = 262.2$ GeV	$m_{\chi_2^0} = 211.7$ GeV	$m_{\chi_3^0} = 155.7$ GeV	$m_{\chi_4^0} = 94.3$ GeV
$N(1,1) = 0.15$	$N(2,1) = -0.10$	$N(3,1) = -0.30$	$N(4,1) = 0.93$
$N(1,2) = -0.70$	$N(2,2) = 0.14$	$N(3,2) = -0.69$	$N(4,2) = -0.10$

Figure 1: Like Sign Dilepton via Drell-Yan sneutrino pair production at an electron or proton collider (for $\ell \neq e$).

Figure 2: Contributions to $e^+e^- \to \tilde{\nu}_l^N \ell^- \tilde{\chi}_i^+$ where N=1,2 and ℓ=μ, τ (for ℓ=e more graphs contribute).

Figure 3: Contributions to $e^+\gamma \to \tilde{\nu}_\ell^N \tilde{\ell}^+ \overline{\nu}_e$. These are the leptonic analogs to single top production in the SM. Graph II containing a four point vertex has no SM-counterpart.

Figure 4: The L violating prefactor ξ^{pair} in sneutrino pair production defined in Eq. (7). The solid lines correspond to parameter set A and (from left to right) $\overline{m}$=120 GeV, 170 GeV, 220 GeV, 300 GeV, 390 GeV; the dashed lines correspond to parameter set B and (from left to right) $\overline{m}$=170 GeV, 220 GeV, 300 GeV, 390 GeV. The parameter sets A and B are defined in Table 1.

Figure 5: LSD cross section at TEVATRON: $\overline{m}$=120 GeV, set A (solid line); $\overline{m}$=170 GeV, set A (dashed line); $\overline{m}$=220 GeV, set A (dot-dashed line); $\overline{m}$=170 GeV, set B (double-dot dashed line); $\overline{m}$=220 GeV, set B (double-dash dotted line). The parameter sets A and B are defined in Table 1.

Figure 6: LSD cross section at LHC for the parameter sets A (left) and B (right) defined in Table 1 for the parameters $\overline{m}$=120 GeV, set A (solid line); $\overline{m}$=170 GeV, set B (solid line); $\overline{m}$=200 GeV, sets A and B (dashed lines); $\overline{m}$=400 GeV, sets A and B (dot-dashed lines); $\overline{m}$=600 GeV, sets A and B (double dot-dashed lines).

Figure 7: LSD cross section in sneutrino pair production at a LC (ℓ=μ, τ) for the parameters: $\overline{m}$=120 GeV, set A, $\sqrt{s}$=500 GeV (solid line); $\overline{m}$=170 GeV, set A, $\sqrt{s}$=500 GeV (dashed line); $\overline{m}$=220 GeV, set A, $\sqrt{s}$=500 GeV (dot-dashed line); $\overline{m}$=170 GeV, set B, $\sqrt{s}$=500 GeV (solid line); $\overline{m}$=220 GeV, set B, $\sqrt{s}$=500 GeV (dashed line); $\overline{m}$=120 GeV, set A, $\sqrt{s}$=800 GeV (solid line); $\overline{m}$=220 GeV, set A, $\sqrt{s}$=800 GeV (dashed line); $\overline{m}$=300 GeV, set A, $\sqrt{s}$=800 GeV (dot-dashed line); $\overline{m}$=390 GeV, set A, $\sqrt{s}$=800 GeV (double dot-dashed line); $\overline{m}$=170 GeV, set B, $\sqrt{s}$=800 GeV (solid line); $\overline{m}$=220 GeV, set B, $\sqrt{s}$=800 GeV (dashed line); $\overline{m}$=300 GeV, set B, $\sqrt{s}$=800 GeV (dot-dashed line); $\overline{m}$=390 GeV, set B, $\sqrt{s}$=800 GeV (double dot-dashed line). The parameter sets A and B are defined in Table 1.

Figure 8: Cross section for chargino-associated sneutrino production depicted in Fig. 2-I and 2-II as a function of the sneutrino mass. The curves correspond to the parameters ($\sqrt{s}$=500 GeV; parameter set A; lower solid line); ($\sqrt{s}$=800 GeV; set A; upper solid line); ($\sqrt{s}$=500 GeV; set B; lower dashed line); ($\sqrt{s}$=800 GeV; set A; upper dashed line). The parameter sets A and B have been defined in Table 1. The sneutrino has been taken to be heavier than the charginos, otherwise the production of two real charginos is allowed and the chargino width must be taken into account.

Figure 9: The L-violating parameter in single sneutrino production ξ^{single} defined in Eq. (13). The varius curves refer to the parameters used in Fig. 10 with the same notation.

Figure 10: Cross section for LSD stemming from the chargino-associated sneutrino production depicted in Fig. 2-I and 2-II. The curves correspond to the parameters $\sqrt{s}$ =500 GeV, $\overline{m}$=275 GeV (parameter set A, upper solid line); $\sqrt{s}$ =500 GeV, $\overline{m}$=350 GeV (set A, lower solid line); $\sqrt{s}$ =800 GeV, $\overline{m}$=450 GeV (set A, upper dashed line); $\sqrt{s}$ =800 GeV, $\overline{m}$=600 GeV (set A, lower dashed line); $\sqrt{s}$ =800 GeV, $\overline{m}$=450 GeV (set B, upper dotted line); $\sqrt{s}$ =800 GeV, $\overline{m}$=600 GeV (set B, lower dotted line). The parameter sets A and B have been defined in Table 1.

Figure 11: cross section for $e^+\gamma \to \tilde{\nu}_\ell^N \tilde{\ell}^+ \overline{\nu}_e$ in a mSUGRA scenario as a function of the common scalar mass M_0, applying the backscattering process (B.S.) Eq. (18) and the equivalent photon approximation (E.P.A) Eq. (19). The curves correspond to the parameters ($\sqrt{s}$=800 GeV, parameter set A; E.P.S.; upper solid line); ($\sqrt{s}$=500 GeV, set A; E.P.S.; lower solid line); ($\sqrt{s}$=800 GeV, set B; E.P.S.; upper long-dashed line); ($\sqrt{s}$=500 GeV, set B; E.P.S.; lower long-dashed line); ($\sqrt{s}$=800 GeV, set A; B.S.; upper dashed line); ($\sqrt{s}$=500 GeV, set A; B.S.; lower dashed line); ($\sqrt{s}$=800 GeV, set B; B.S.; upper dotted line); ($\sqrt{s}$=500 GeV, set B; B.S.; lower dotted line). The parameter sets A and B have been defined in Table 1 (the center of mass energy refers to the electron-positron beam).

Figure 12: cross section for the wrong sign charged lepton signal stemming from $e^+\gamma \to \tilde{\nu}_\ell^N \tilde{\ell}^+ \overline{\nu}_e$ (in a mSUGRA scenario) as a function of the ratio $\Delta m/\overline{m}$ applying the backscattering process (B.S.) Eq. (18) and the equivalent photon approximation (E.P.A) Eq. (19). The curves correspond to ($\sqrt{s}$=500 GeV, M_0=100 GeV; parameter set A; E.P.S.; upper solid line); ($\sqrt{s}$=500 GeV, M_0=100 GeV; set A; B.S.; lower solid line); ($\sqrt{s}$=800 GeV, M_0=300 GeV; set A; E.P.S; upper dashed line); ($\sqrt{s}$=800 GeV, M_0=300 GeV; set A; B.S.; lower dashed line); ($\sqrt{s}$=800 GeV, M_0=300 GeV; set B; E.P.S; upper dotted line); ($\sqrt{s}$=800 GeV, M_0=300 GeV; set B; B.S.; lower dotted line). The parameter sets A and B have been defined in Table 1. For M_0=100 GeV the data is cut off where the lighter sneutrino becomes lighter than the LSP, the bump corresponds to the value of Δm where the heavier sneutrino is not produced any more.

Figure 13: cross section for the wrong sign charged lepton signal stemming from $e^+\gamma \to \tilde{\nu}_\ell^N \tilde{\ell}^+ \overline{\nu}_e$ as a function of the ratio $\Delta m/\overline{m}$ applying the backscattering process (B.S.) Eq. (18). No mSUGRA conditions were assumed. The curves correspond to ($\sqrt{s}$=500 GeV, $\overline{m}$=200 GeV; $m_{\tilde{\ell}}$=100 GeV; parameter set A; B.S.; solid line); ($\sqrt{s}$=800 GeV, $\overline{m}$=300 GeV; $m_{\tilde{\ell}}$=200 GeV; parameter set A; B.S.; dashed line); The parameter set A has been defined in Table 1.

Figure 14: Cross section of the LSD signal in single sneutrino production at an electron collider Eq. (12) for the case of a very small common sneutrino width Γ :=Γ_1=Γ_2= $\Gamma_1(\chi^\pm \ell^\mp)$= $\Gamma_2(\chi^\pm \ell^\mp)$ and for the and for the parameters (set A; $\sqrt{s}$=500 GeV; $\overline{m}$=275 GeV) in dependence of Δm (in GeV). The solid line corresponds to Γ=10 MeV, the dashed line corresponds to Γ=1 MeV and the dot-dashed line to Γ=100 keV. For a neutrino mass of order $\mathcal{O}$(1 eV) ($\Delta m \approx 200\,\text{keV} = 2\times10^{-4}$ GeV, see Eq. 22) the LSD is of order $\mathcal{O}$(0.01 fb) (dashed line).

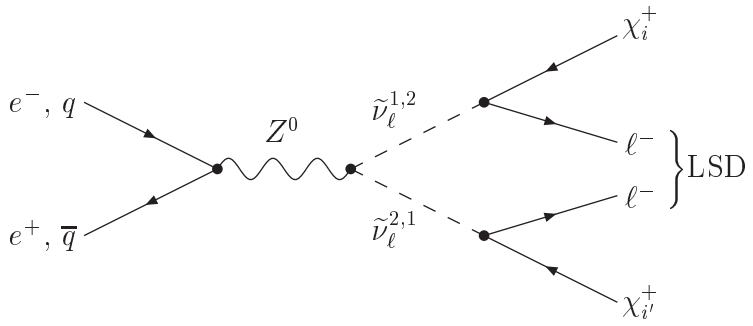

Fig. 1

Kolb *et al.*

Physical Review D

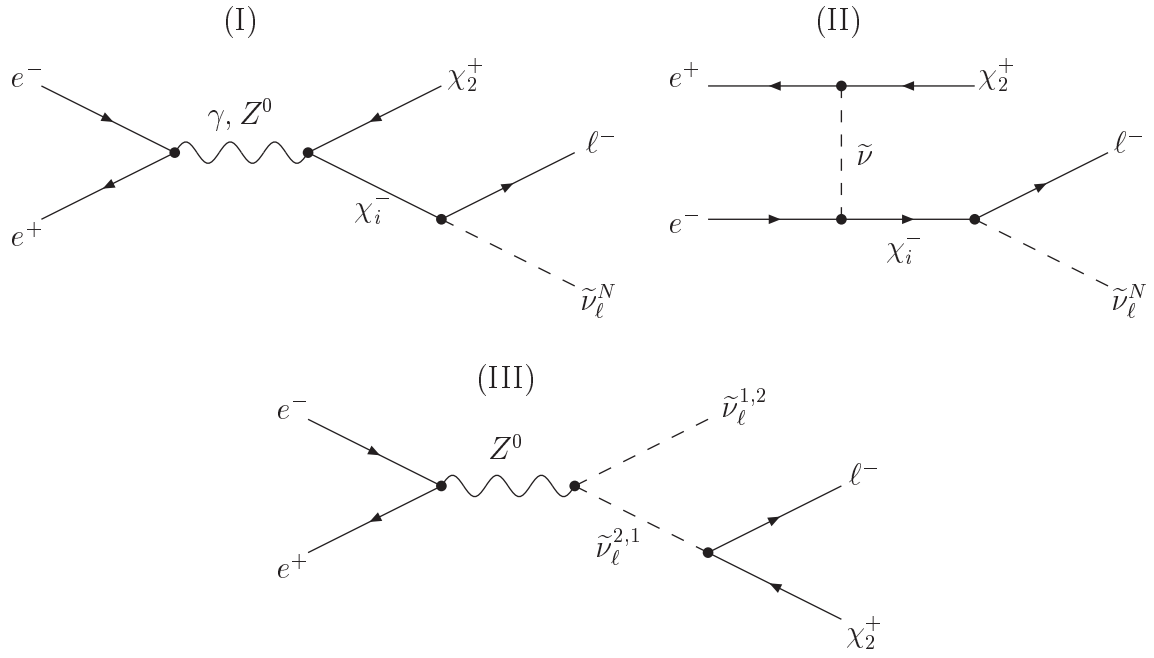

Fig. 2

Kolb *et al.*

Physical Review D

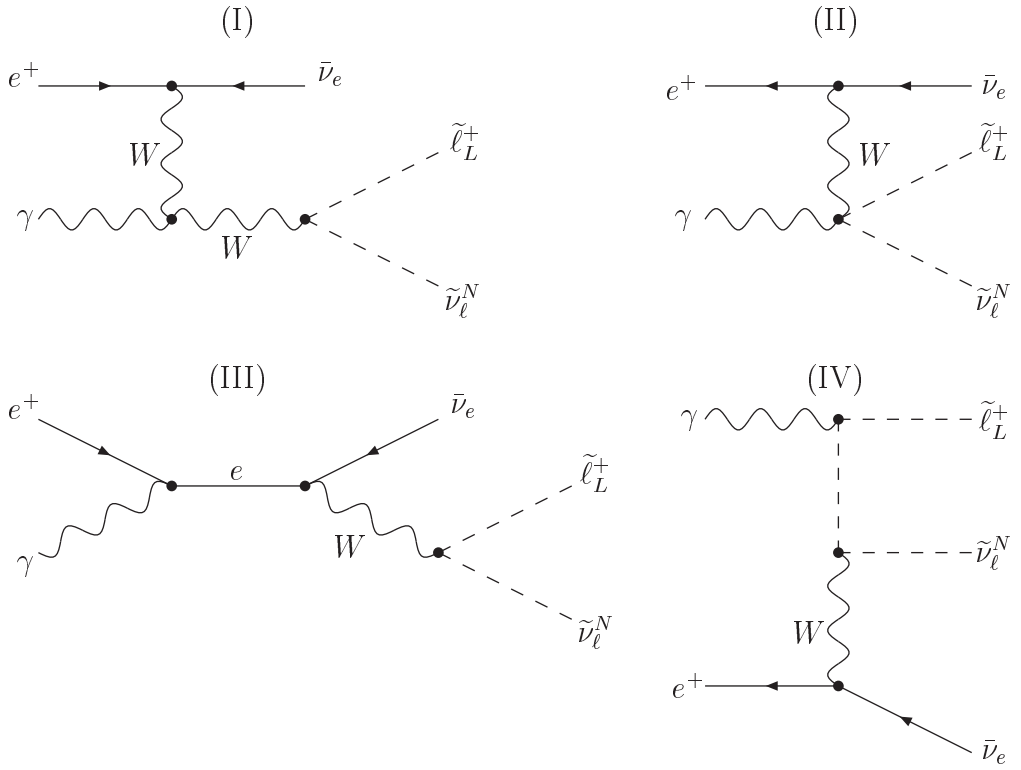

Fig. 3

Kolb *et al.*

Physical Review D

Fig. 4

Kolb et al.

Physical Review D

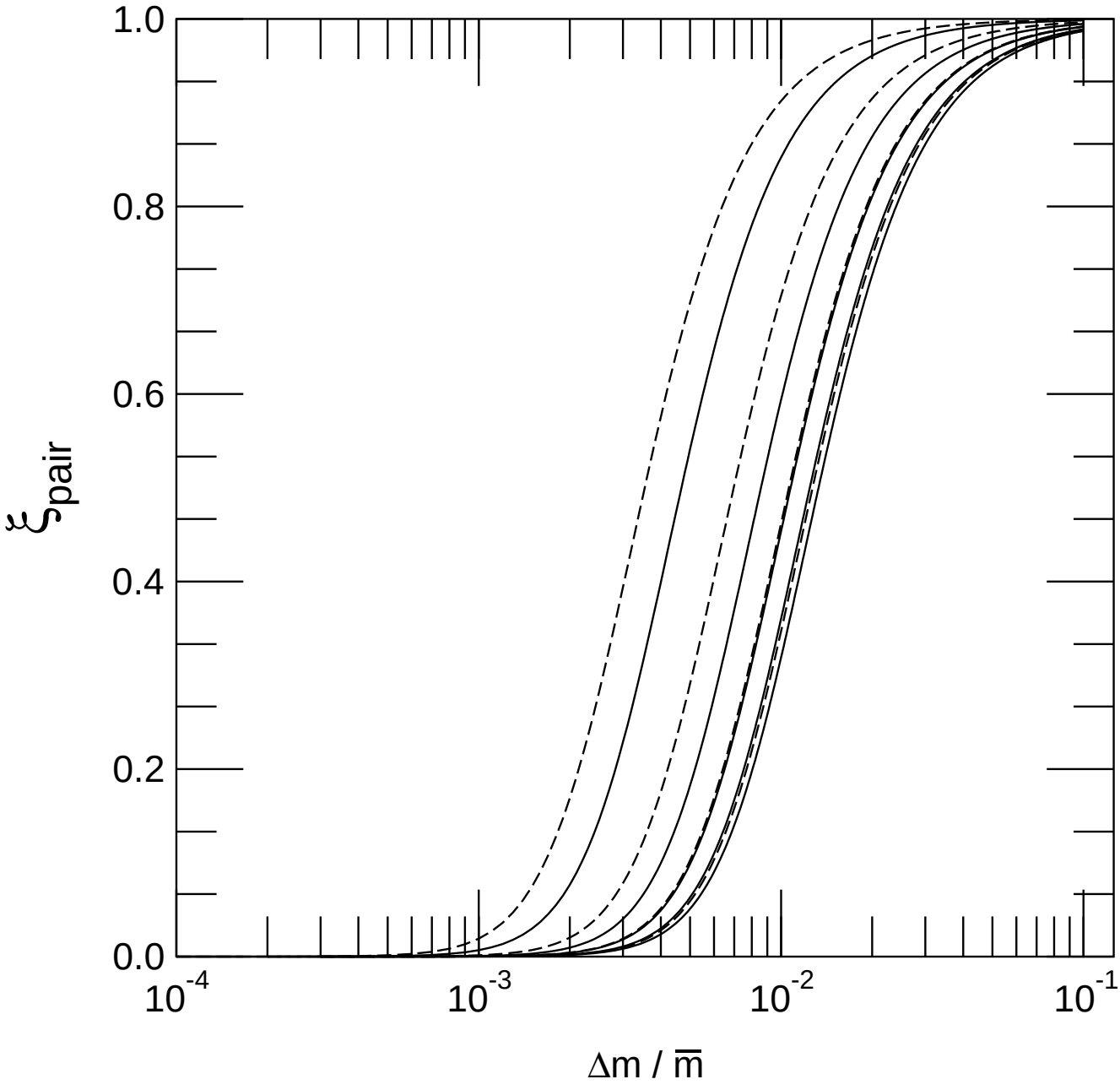

Fig. 5

Kolb et al.

Physical Review D

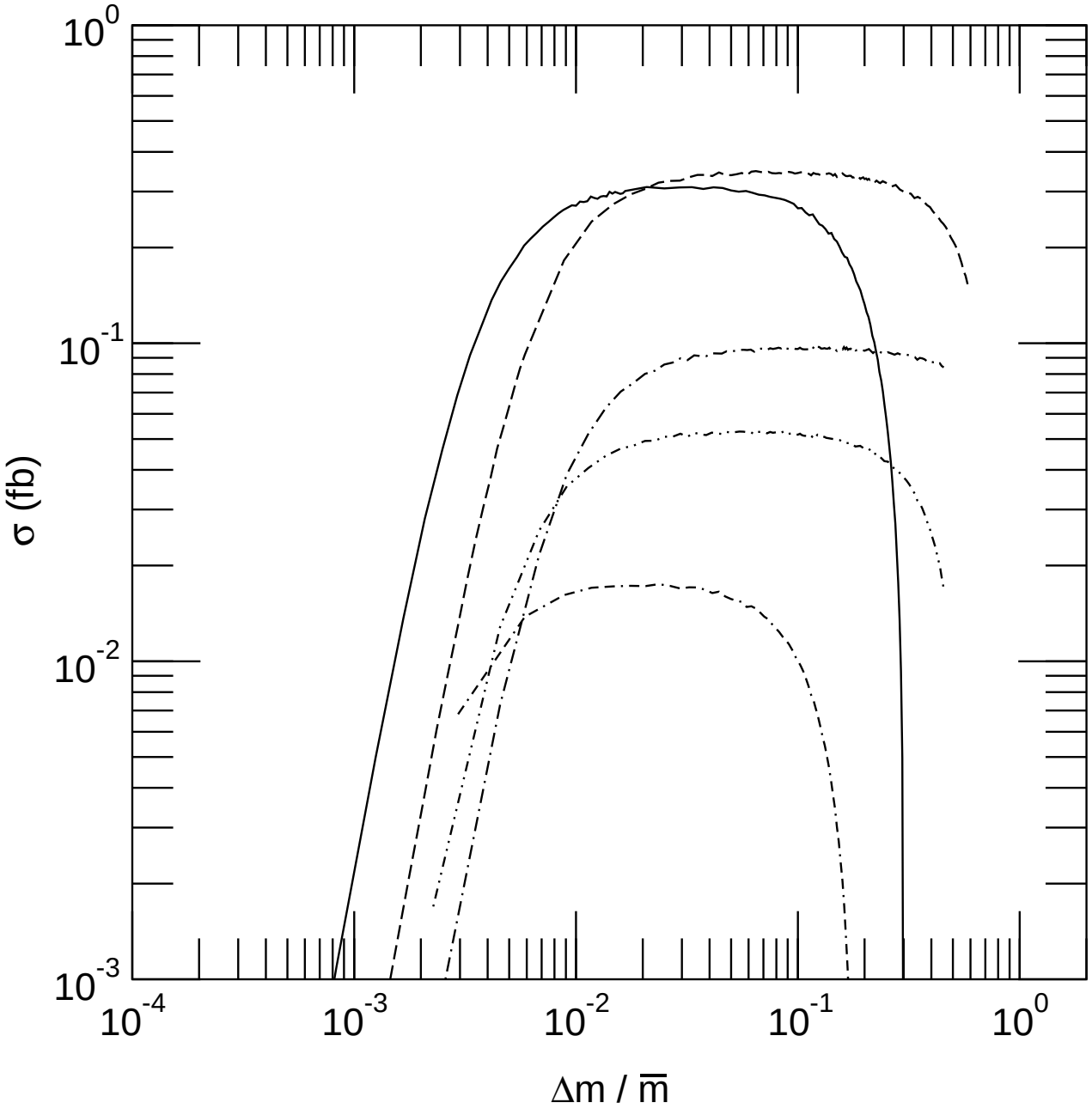

Fig. 6

Kolb et al.

Physical Review D

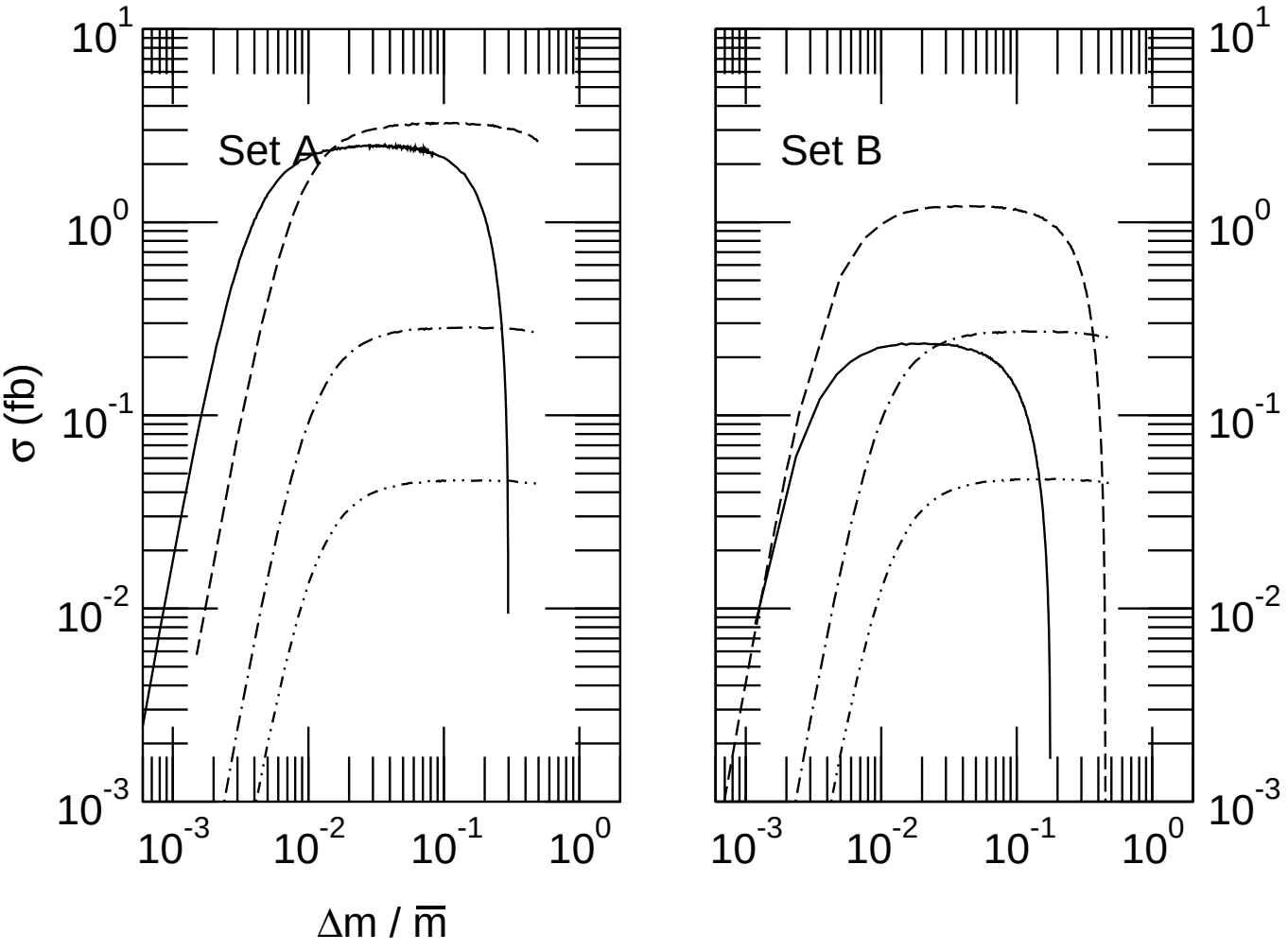

Fig. 7

Kolb et al.

Physical review D

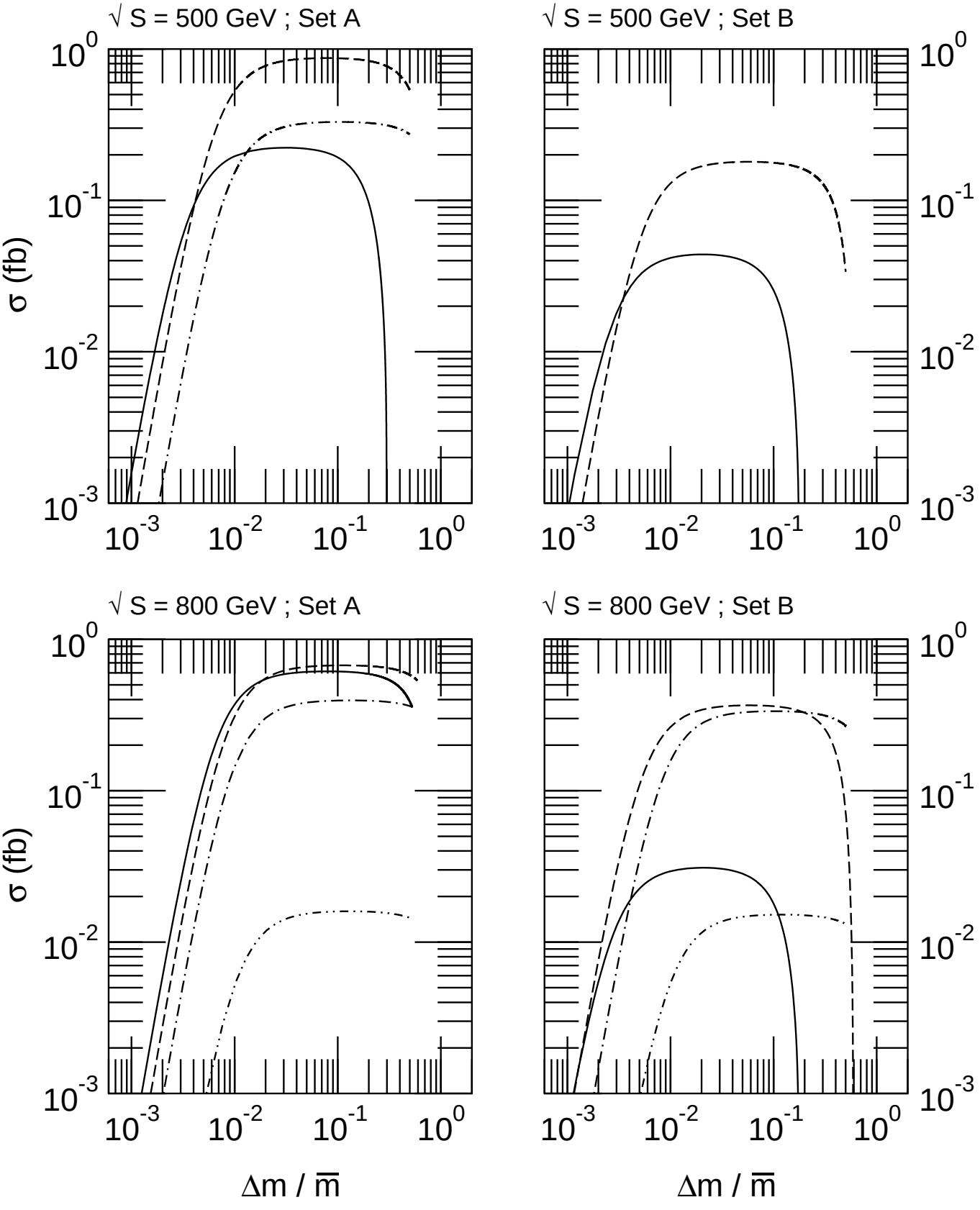

Fig. 8

Kolb et al.

Physical Review D

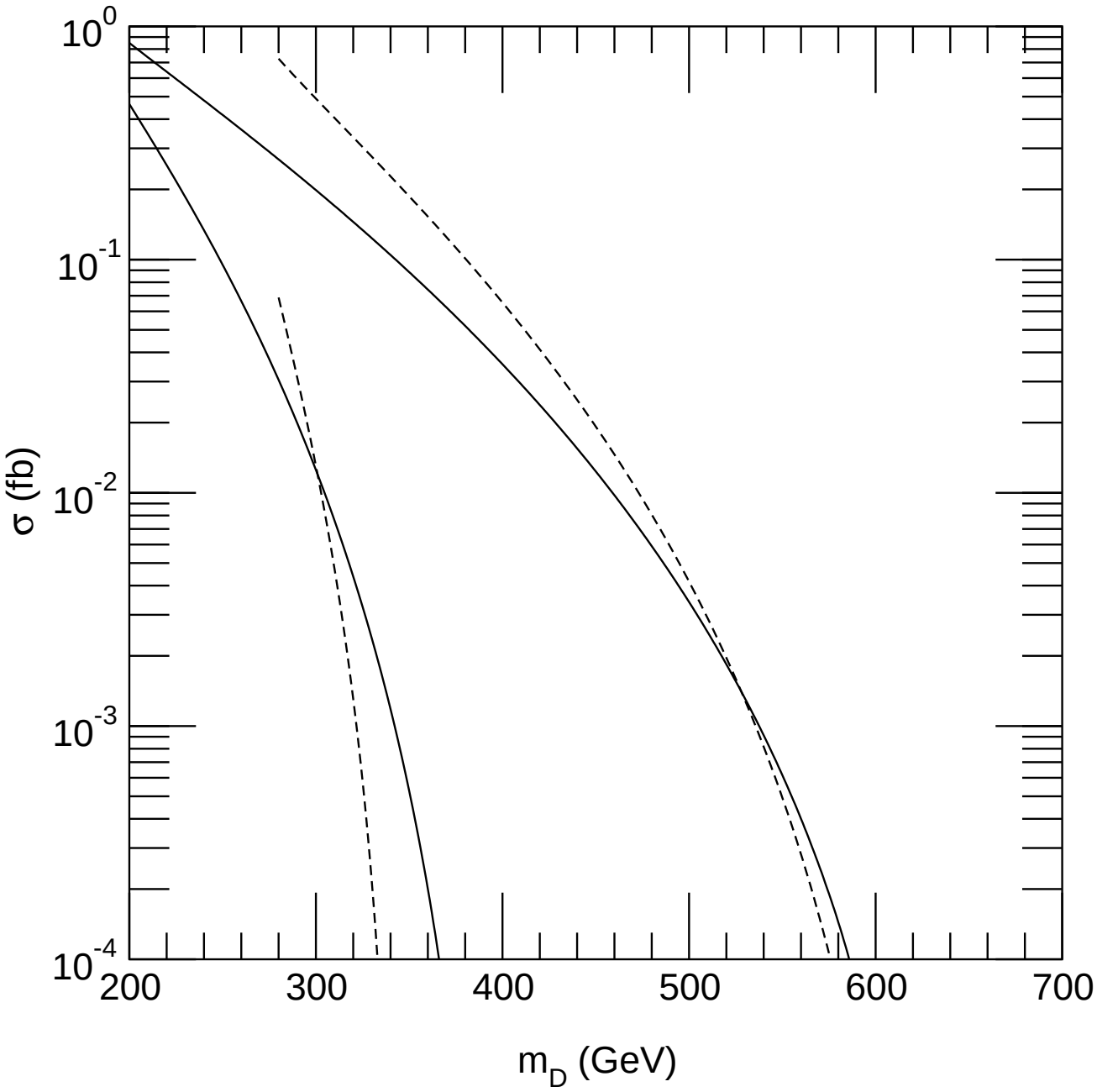

Fig. 9

Kolb et al.

Physical Review D

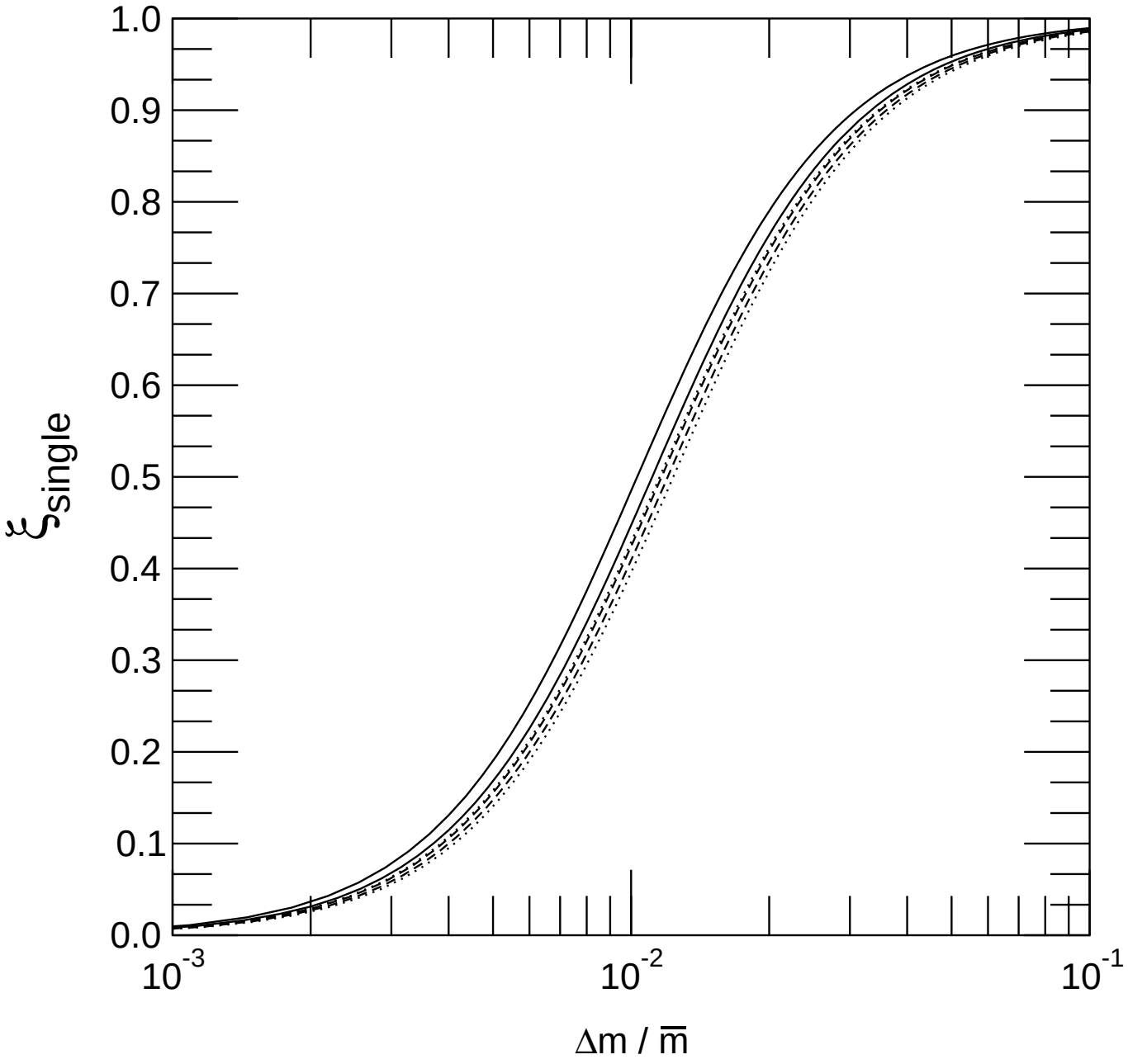

Fig. 10

Kolb et al.

Physical Review D

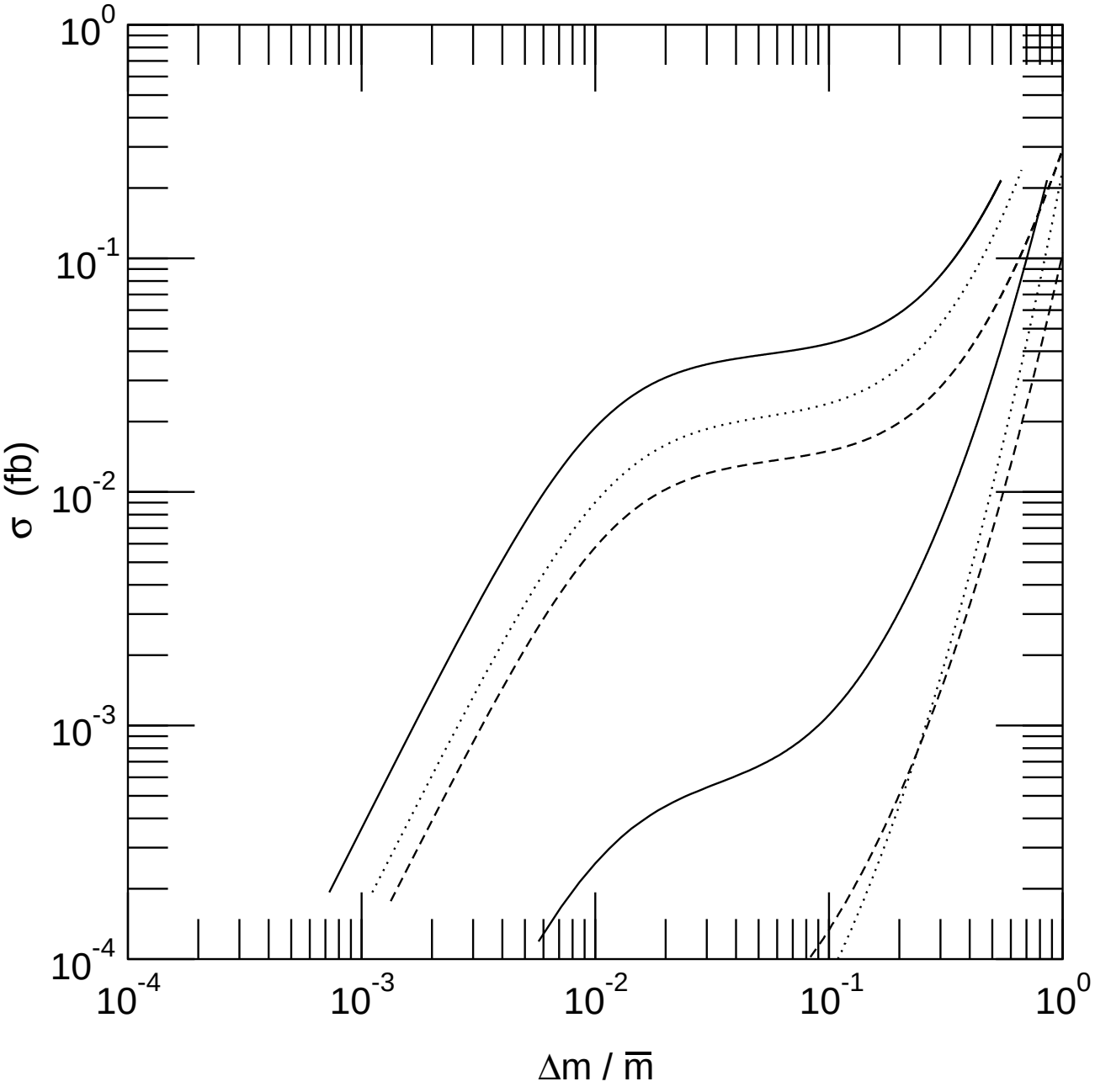

Fig. 11

Kolb et al.

Physical Review D

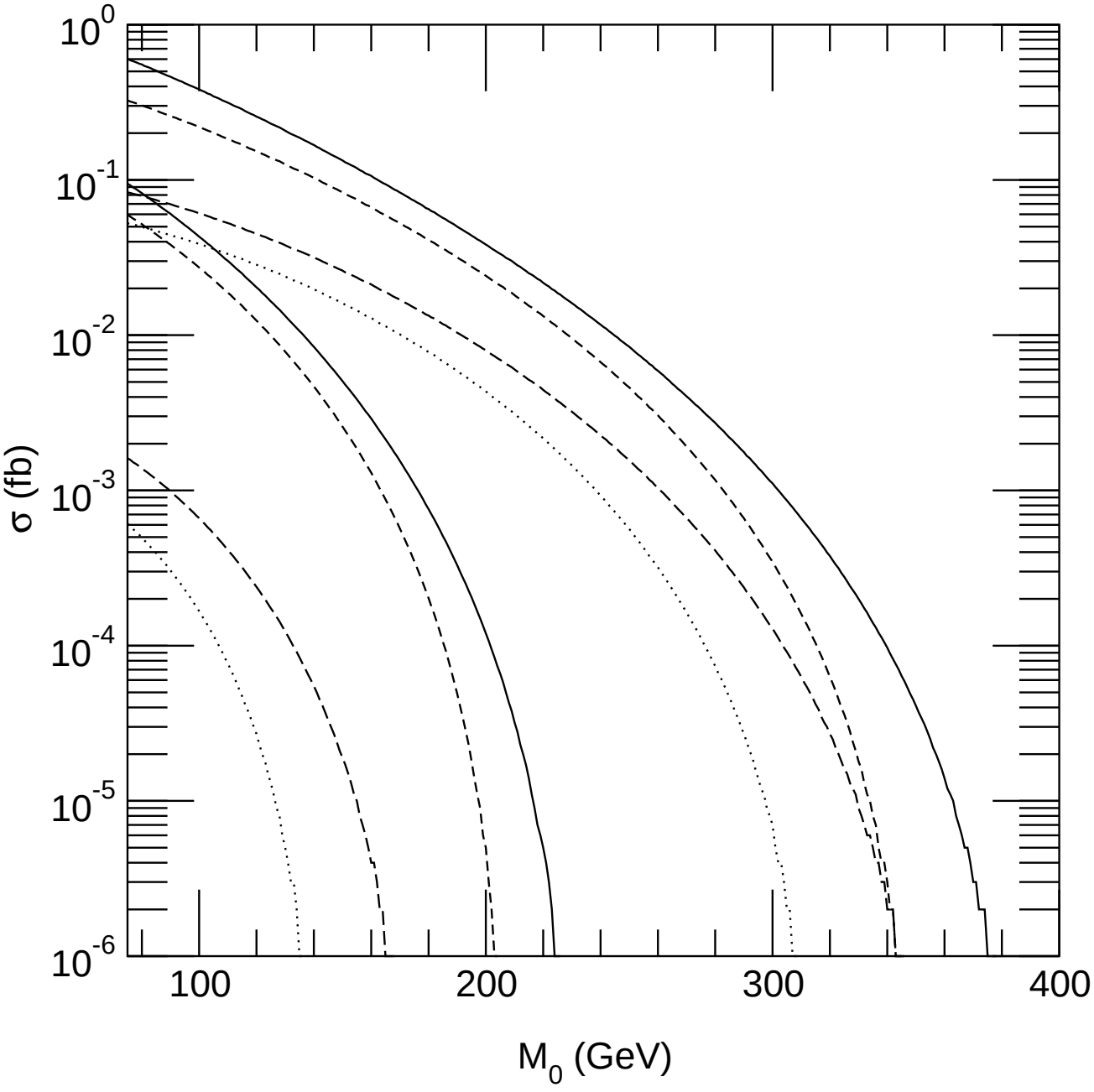

Fig. 12

Kolb et al.

Physical Review D

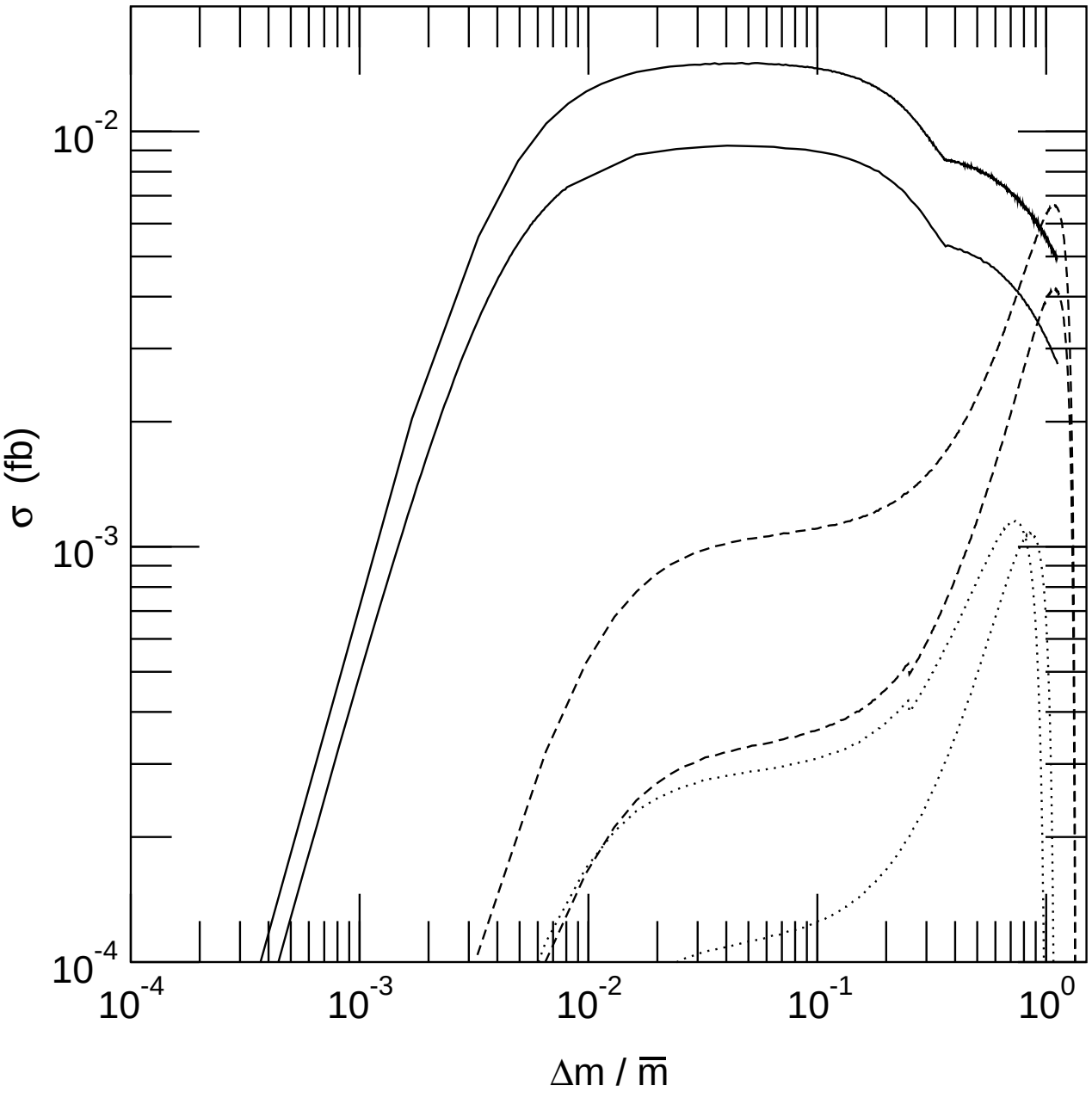

Fig. 13

Kolb et al.

Physical Review D

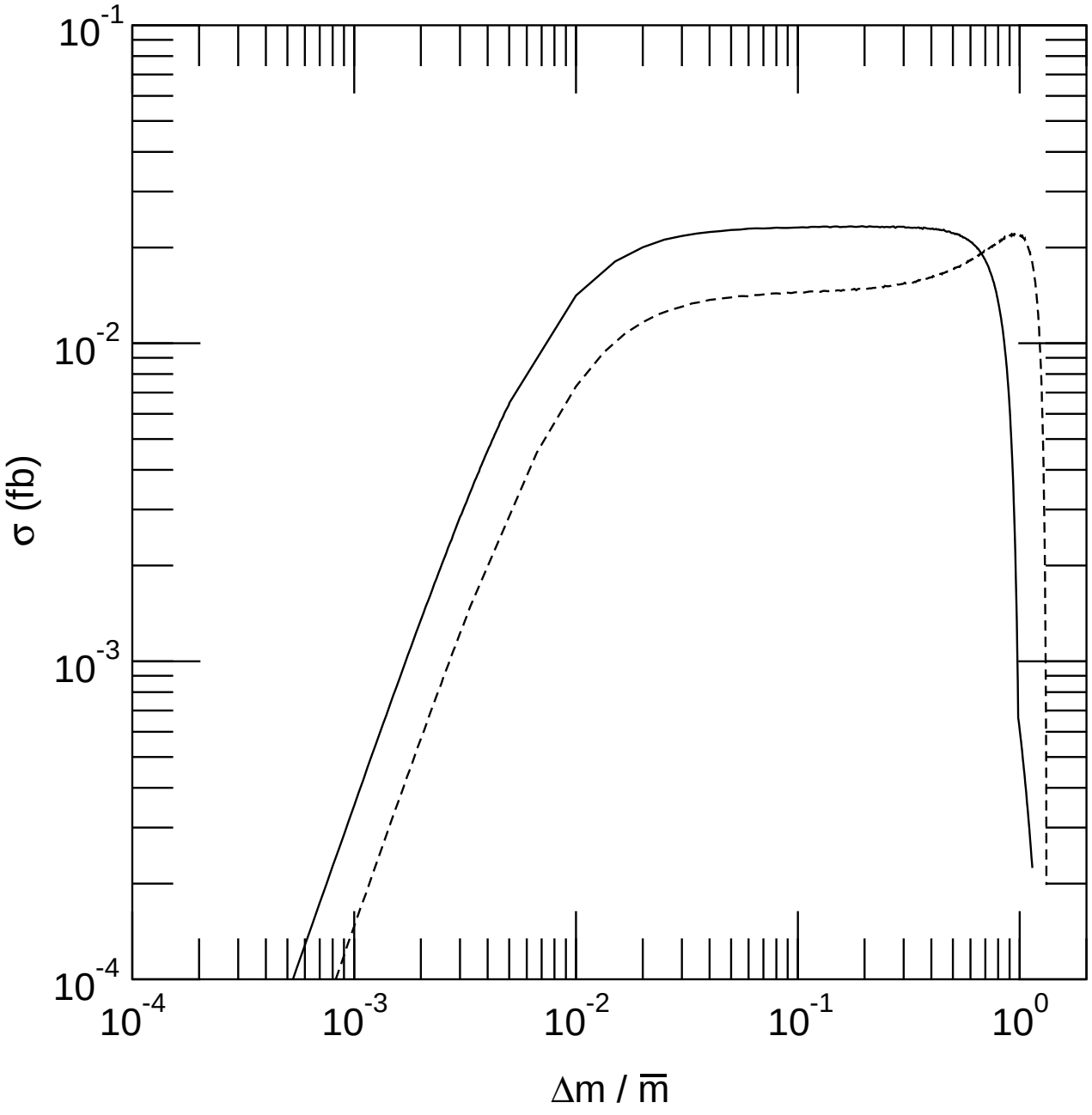

Fig. 14

Kolb et al.

Physical Review D